An enhanced PDEM-based framework for reliability analysis of structures considering multiple failure modes and limit states

De-Cheng Feng[a], Xu-Yang Cao[b,*], Michael Beer[c,d,e]

[a]*Key Laboratory of Concrete and Prestressed Concrete Structures of the Ministry of Education, Southeast University, Nanjing 210096, China*
[b]*College of Civil and Transportation Engineering, Hohai University, Nanjing 210098, China*
[c]*Institute for Risk and Reliability, Leibniz University Hannover, Callinstr. 34, Hannover, Germany*
[d]*Institute for Risk and Uncertainty, University of Liverpool, Peach Street, L69 7ZF Liverpool, United Kingdom*
[e]*International Joint Research Center for Resilient Infrastructure & International Joint Research Center for Engineering Reliability and Stochastic Mechanics, Tongji University, Shanghai 200092, China*

Abstract

In this paper, an enhanced probability density evolution method (PDEM) framework considering multiple failure modes and limit states is proposed for reliability analysis of structures. Firstly, the PDEM principle and the enhanced mechanism are illustrated, and during the process three typical combination types (i.e., circle, triangle, square ways) are introduced. Secondly, two case studies are given to verify the effectiveness of the enhanced PDEM-based framework and the necessity to consider multiple limit states. The first example is a simply supported beam under two-point concentrated forces with two failure conditions (i.e., shear failure and flexural failure), and the second example is a 3-span-6-story reinforced concrete frame under seismic excitation with three failure conditions (i.e., maximum displacement failure, residual displacement failure and floor acceleration failure). Meanwhile, the Monte Carlo simulation (MCS) is also performed for both examples as a comparison and validation. Thirdly, parametric studies with related to two important aspects in the enhanced PDEM-based framework are primarily performed, including a modified equation of the target variable value via representative points incorporating the influence of individual quantile parameters (e.g., 16%, 50% and 84% quantile), as well as the other potential combination types in the enhanced PDEM-based framework (i.e., more than circle, triangle, square ways). In general, the paper provides a reference to perform the PDEM-based reliability assessment for multiple limit states and multiple failure patterns in the future. The enhanced framework presents less calculation burden and shows comparative calculation accuracy with the MCS. Meanwhile, the enhanced results are generally more conservative and commonly illustrate a lower reliability when compared with the single limit state, which can result in a more comprehensive decision and more robust strategy under the same condition in the practical engineering.

Keywords: Limit state functions, Structural failure modes, Reliability, Probability, Multiple, Structural assessment, PDEM framework

1. Introduction

In the performance assessment framework of engineering structures, how to define the failure mode and corresponding threshold is a critical step [1, 2, 3]. An appropriate selection of failure condition and proper determination of damage measure can give a more comprehensive conclusion of structural behaviors, which simultaneously provides a beneficial effect for further optimal strategy and appropriate decision making [4]. The judgement of structural failure boundary is commonly related to the limit state function (LSF) [5], and two physical variables are generally involved during the analysis, i.e., structural resistance (R) and response (S). In the deterministic theory, when the response is smaller than resistance, i.e., LSF=S-R<0, the structural system is regarded to be safe or reliable, while when the response exceeds resistance, i.e., LSF=S-R>0, the structural system is regarded to be damaged in failure. At this stage, the LSF has been extended to various sub-fields of civil engineering, e.g., in the earthquake engineering, resistance and response can be rephrased as capacity and demand, and LSF is further connected to the fragility analysis for performance evaluation. Under this background, the investigation of structural LSF or failure modes has become a research interest for decades, and the development is continuing with rapid progress [6, 7, 8].

The traditional performance assessment adopts the single failure condition and damage measure to analyze. For instance, in the classic force-based design of concrete components, the single failure relationship or LSF between flexural resistance and flexural response is commonly used as a criterion. Another example is that in the performance-based design of engineering structures through lateral displacement, the single failure relationship or LSF between maximum drift ratio resistance and maximum drift ratio response is primarily selected as a criterion. However, according to Cimellaro and Reinhorn [9], the performance level of an integrated structure is commonly decided by multiple limit states and controlled by multiple failure modes. Take the above examples again, in the force-based design of concrete components, shear failure may happen before the flexural failure, thus the shear mode is also an important factor which is required consideration simultaneously [10, 11]. In the displacement-based design of engineering structures, residual deformation may be too large to repair after seismic events, even though the maximum deformation satisfies within the requirement. Thus, residual deformation is also an important factor which deserves consideration in the design procedure [12, 13]. In another word, adopting only single limit state or single failure condition may underestimate the structural failure potential, and a more radical conclusion may be drawn [14, 15]. The influence of multiple limit states and various failure modes in structural behavior assessment has aroused attention by researchers [16, 17, 18].

In 2001, Estes and Frangopol [19] performed the reliability assessment of bridge life-cycle system considering multiple limit states, and both the ultimate and serviceability limit states were considered to give a

*Corresponding author.
Email addresses: dcfeng@seu.edu.cn (De-Cheng Feng), caoxy@hhu.edu.cn (Xu-Yang Cao), beer@irz.uni-hannover.de (Michael Beer)

more overall performance strategy of bridges in the lifetime. In 2007, Mackie and Stojadinovi [20] provided a non-iterative performance-based seismic design approach considering multiple damage and loss limit states, and during the analysis, multiple physical design parameters were incorporated to compare the uncertainty source and to derive the design equation under different performance objectives. In 2010, Orcesi et al. [21] optimized the maintenance strategies of engineering structures based on multiple limit states (i.e., force-level states and function-level states), and the corresponding influence in different maintenance decisions resulted from multiple limit states were well discussed and analyzed. In 2011, Cimellaro and Reinhorn [9] addressed a seismic fragility approach in light of multiple limit states parameters, and a generalized multidimensional LSF containing dependencies among limit thresholds was defined, which provided an alternative path to describe structural fragile behaviors with multiple parameters sensitivity (e.g., combined accelerations and displacements limit states). In 2017, Biondini and Frangopol [22] investigated the multiple failure loads and destruction times of concrete structures under the corrosion condition, and two case studies (i.e., reinforced concrete frame and bridge deck) were given to illustrate the effectiveness of proposed approach in defining the suitable performance levels of serviceable life-cycle. In 2019, Mojtabaei et al. [23] developed the optimisation strategy of cold-formed steels considering multiple ultimate and serviceability limit states, and both the maximum flexural strength factor and minimum deflection factor were incorporated during the performance evaluation. The results indicated a higher effective stiffness and bending moment capacity (varing from 44% to 58%) in comparison with a standard lipped channel beam, under the consideration of multiple limit states and optimisation algorithm. In 2021, Valdebenito et al. [24] adopted the multi-domain line sampling to calculate the system failure probability, and multiple limit states were considered simultaneously. The failure domain information of single component was exploited, and the influence of interactions between failure events was well discussed. In 2022, Sohn et al. [25] proved the inadequacy of existing single limit state for typical piloti-type buildings through correlation analysis, and further proposed a combined strain-based and drift-ratio-based limit state to reflect the local damage caused by vertical irregularity, which was validated with the collected damage data.

On the other hand, the traditional LSF analysis commonly gives an instantaneous evaluation of structural behavior under the deterministic condition, and with the development of uncertainty theory, the LSF is further connected to probability in the field of uncertainty, among which the reliability assessment is a significant sub-division [26, 27, 28, 29, 30]. At this stage, a great many reliability assessment approaches have been well developed (e.g., checking point method [31], central point method [32], boundary estimation method [33], probability network estimation [34], Monte Carlo approach [35], etc., and the corresponding explanations as well as the typical applications can be found in [36, 37, 38, 39, 40, 41, 42]). As an alternative approach, the probability density evolution method (PDEM), which contains verified theoretical basis and solid mathematical derivations in the reliability community, has been proposed by Li et al. since 2000s [43, 44, 45, 46]. Without the predefined types of distribution for the target random variables, the PDEM approach partitions the random space with different assigned probability (e.g., via optimal minimum F-Discrepancy method proposed by Li and Chen [47, 48]) and gives the evolutional tendency of the target random variables via efficient numerical difference strategy [e.g., Lax-Wendroff (L-W) form or total variation (TV) form [49]]. Compared with the classic Monte Carlo approach, the PDEM approach reduces the calculation burden aggressively and keeps the calculation accuracy effectively [50, 51]. Moreover, the obtained reliability trends indicate the non-parametric characteristics, thus can better reflect the real stochastic conditions in the practical engineering [52, 53]. The development of PDEM approach has been further propelled by researchers in recent ten years.

In 2016, Xu [54] performed the stochastic dynamic stability analysis of structures with viscoelastic dampers via the enhanced PDEM-based approach, and during the period, newly developed criteria were included into the PDEM framework to identify the stable/unstable properties of the dynamic system. Numerical examples were also given to illustrate the efficiency and effectiveness of the approach. In 2017, Fan et al. [55] combined the Bayesian updating with the PDEM approach for deteriorating structures, and the changes of probabilistic information as well as the numerical solution via PDEM were well derived. Two numerical examples were discussed correspondingly, indicating that the modified PDEM framework with Bayesian updating was rational and accurate. In 2019, Hu and Huang [56] incorporated the random field theory into the traditional framework of PDEM, and the spatially variable soil properties were regarded as the target physical objects. The soil uncertainty propagations and sensitivity analyses in the dynamic system were well discussed to verify the superiority of the improved approach. In 2020, Feng et al. [57] proposed a reliability-based framework for the robustness quantification of reinforced concrete (RC) structures under progressive collapse, and the PDEM with the equivalent extreme value event was well incorporated to capture the reliability indices during the whole collapse process. The reliability results were compared with the Monte Carlo simulation, and the data reflected the distinctively improved calculation efficiency and the ideal reliability accuracy of the proposed PDEM approach. In 2020, Wan et al. [58] proposed a new lifetime reliability assessment approach by combining the PDEM with the probability measure change, and three case studies were given to verify the effectiveness of the proposed method. In 2021, Chen et al. [59] considered the time-varying factors in the PDEM-based dynamic reliability method, and successfully applied them into the seismic assessment of a concrete dam subjected to earthquakes. The proposed framework was proved to be efficient for complex structures, and meanwhile showed great potentials for the lifetime seismic design in the future. In 2021, Zhou and Peng [60] incorporated the active learning and subspace improvement technique into the PDEM for high-dimensional reliability analysis, and the results indicated that the proposed approach outperformed other existing reliability approaches.

Although researchers have progressed the PDEM theory in the reliability field from new influential factors to new application scenarios as mentioned above, the study on how to appropriately combine the multiple limit states within the PDEM-based framework and how to incorporate the multiple structural failure modes for PDEM-based reliability assessment is relatively scarce, which deserves further exploration in depth. Thus, in this paper, an enhanced PDEM-based framework considering multiple failure modes and limit states is proposed for reliability analysis of structures. Firstly, the PDEM principle and the enhanced mechanism are illustrated, and during the process three typical combination types (i.e., circle, triangle, square ways) are introduced. Secondly, two case studies are given to verify the effectiveness and necessity of the enhanced PDEM-based framework considering multiple limit states. The first example is a simply supported beam under two-point concentrated forces with two failure conditions (i.e., shear failure and flexural failure), and the second example is a 3-span-6-story RC frame under seismic excitation with three failure conditions (i.e., maximum displacement failure, residual displacement failure and floor acceleration failure). Meanwhile, the Monte Carlo simulation (MCS) is also performed for both examples as a comparison and validation. Thirdly, parametric studies with related to two important aspects in the enhanced PDEM-based framework are primarily performed, including a modified equation of the target variable value via representative points incorporating the influence of individual quantile parameters (e.g., 16%, 50% and 84% quantile), as well as the other potential combination types in the enhanced PDEM-based framework (i.e., more than circle, triangle, square ways illustrated in this paper). The detailed contents of the above-mentioned three parts are elaborated from Sections 2 to 4, respectively.

2. Enhanced PDEM framework for reliability analysis

2.1. Principle of probability density evolution method

The well-known PDEM is introduced in this section, and an enhanced framework considering multiple LSFs and multiple structural failure modes is further proposed for reliability analysis. According to Li et al. [43, 44], the PDEM possesses solid theoretical basis and verified mathematical derivations in the reliability field. Without the loss of generality, a structural system commonly contains multiple stochastic capacity parameters [e.g., materials, dimensions, herein expressed as $\boldsymbol{\Theta_c} = (\boldsymbol{\Theta}_1, \boldsymbol{\Theta}_2, ..., \boldsymbol{\Theta}_e)^T$] and multiple loading parameters [e.g., phase angles, action points, herein expressed as $\boldsymbol{\Theta_l} = (\boldsymbol{\Theta}_{e+1}, \boldsymbol{\Theta}_{e+2}, ..., \boldsymbol{\Theta}_n)^T$]. For simplicity, the random vector $\boldsymbol{\Theta} = (\boldsymbol{\Theta}_c, \boldsymbol{\Theta}_l)$ is defined, which includes n groups of independent $m \times 1$ sub-matrices, where m denotes the samples for each stochastic variable. Meanwhile, for each realizable value of random vector $\boldsymbol{\Theta}$, the dynamic-motion balance equation of an arbitrary structural system can be expressed as (Eq. 1):

$$\boldsymbol{M}\ddot{\boldsymbol{H}}(\boldsymbol{\Theta}, t) + \boldsymbol{C}\dot{\boldsymbol{H}}(\boldsymbol{\Theta}, t) + \boldsymbol{K}\boldsymbol{H}(\boldsymbol{\Theta}, t) = -\boldsymbol{M}\ddot{h_g}(\boldsymbol{\Theta},\ t) \tag{1}$$

where $\boldsymbol{M}$, $\boldsymbol{C}$ and $\boldsymbol{K}$ are the mass, damping and stiffness matrices of the integrated system with the dimension of $m \times n$, respectively. $\ddot{\boldsymbol{H}}(\boldsymbol{\Theta}, t)$, $\dot{\boldsymbol{H}}(\boldsymbol{\Theta}, t)$ and $\boldsymbol{H}(\boldsymbol{\Theta}, t)$ are the acceleration, velocity and displacement matrices of the integrated system with the dimension of $m \times 1$, respectively. $\ddot{h}_g(\mathbf{\Theta},\ t)$ is the external excitation or dynamic input.

In Eq. 1, the system randomness is only depicted by $\mathbf{\Theta}$, and more generally, $\boldsymbol{H}(\mathbf{\Theta}, t)$ can be expressed as any quantity of interest or concerned physical object of the integrated system, relying on each $\mathbf{\Theta}$. Then, in light of the probability preservation theorem, the generalized density evolution equation (GDEE) of PDEM for a specific demand $\boldsymbol{H}(\mathbf{\Theta}, t)$ is called for, as shown in Eq. 2:

$$\frac{\partial p_{\boldsymbol{H}\mathbf{\Theta}}(\boldsymbol{H},\ \mathbf{\Theta},\ t)}{\partial t} + \dot{\boldsymbol{H}}(\mathbf{\Theta}, t) \cdot \frac{\partial p_{\boldsymbol{H}\mathbf{\Theta}}(\boldsymbol{H},\ \mathbf{\Theta},\ t)}{\partial \boldsymbol{H}} = 0 \tag{2}$$

where t is the generalized time indicating the direction of probability evolution, and $p_{\boldsymbol{H}\mathbf{\Theta}}(\boldsymbol{H},\ \mathbf{\Theta},\ t)$ is the joint probability density function (PDF) of $(\boldsymbol{H},\ \mathbf{\Theta})$. In the implementation process, the Eq. 2 is solved by finite difference methods [e.g., Lax-Wendroff (L-W) form or total variation (TV) form [49]], considering the complicated dynamic behaviors of target variable $\boldsymbol{H}(\mathbf{\Theta}, t)$ and un-explicit form via analytical approach. Besides, the probability-assigned space of $\mathbf{\Theta}$ is needed to be partitioned (i.e., $\Omega_{\mathbf{\Theta}}$), and a series of representative point sets are generated through an optimal minimum F-Discrepancy method proposed by Li and Chen [47, 48]. During the procedure, the probability preservation theorem is satisfied. Then, the initial condition of the integrated system is introduced, as expressed in Eq. 3:

$$p_{\boldsymbol{H}\mathbf{\Theta}}(\boldsymbol{H},\ \mathbf{\Theta},\ t)|_{t=t_0} = \delta(\boldsymbol{H} - \boldsymbol{H}_0) p_{\mathbf{\Theta}}(\mathbf{\Theta}) \tag{3}$$

where $\delta(\cdot)$ is the classic Dirac function, and $\boldsymbol{H}_0$ is the deterministic response of the quantity of interest at the initial time (t_0). $p_{\mathbf{\Theta}}(\mathbf{\Theta})$ denotes the PDF of random vector $\mathbf{\Theta}$, and for the discrete variable, it is converted into the partitioned space with different assigned probability, namely, $P_{\mathbf{\Theta}}(\mathbf{\Theta})$. Afterwards, the PDF of the quantity of interest $[p_{\boldsymbol{H}}(\boldsymbol{H}, t)]$ at the generalized time t can be expressed as (Eq. 4) along the probability evolution direction:

$$p_{\boldsymbol{H}}(\boldsymbol{H}, t) = \int_{\Omega_{\mathbf{\Theta}}} p_{\boldsymbol{H}\mathbf{\Theta}}(\boldsymbol{H},\ \mathbf{\Theta},\ t) d\mathbf{\Theta} \tag{4}$$

With the PDF results of $p_{\boldsymbol{H}}(\boldsymbol{H}, t)$, the cumulative distribution function (CDF) of quantity of interest $[F_{\boldsymbol{H}}(\boldsymbol{H}, t)]$ can be acquired as Eq. 5:

$$F_{\boldsymbol{H}}(\boldsymbol{H}, t) = \int p_{\boldsymbol{H}}(\boldsymbol{H}, t) \cdot d\boldsymbol{H} \tag{5}$$

Worth mentioning herein is that t represents the generalized time, thus it can also reflect the virtual time in analysis. In this condition, an equivalent extreme-value event or virtual stochastic process is established in PDEM, and the virtual time t is assumed to increase from 0 to 1. The quantity of interest $p_{\boldsymbol{H}}(\boldsymbol{H}, t)$ in Eq. 4 can be characterized as the extreme values of structural system (e.g., maximum interstory drift ratio, maximum shear capacity, peak floor acceleration). Through generating the equivalent extreme-value event or virtual stochastic process, the extreme value in each probability space is constructed to appear at the virtual time $t = 1$. After obtaining the PDEM-based PDF and CDF of the extreme value, the corresponding reliability or failure probability of the structural system can be handled subsequently.

To calculate the system reliability when several limit states are considered, say, totally α limit states, the system reliability (R) can then be denoted in Eq. 6:

$$R = F\left\{\bigcup_{i=1}^{\alpha}\{L_i(\boldsymbol{\Theta}, t) > 0, t \in [0, t_i]\}\right\} \tag{6}$$

where $F\{\cdot\}$ denotes the probability under the considered event, i denotes the ith limit state, $L_i(\cdot)$ denotes the ith LSF, and $[0, t_i]$ denotes the time domain for the ith limit state. Then calling for the virtual stochastic process for the equivalent extreme-value analysis, as expressed in Eq. 7:

$$\boldsymbol{T_{ev}} = max\left\{min[L_i(\boldsymbol{\Theta}, t)]\right\}, 1 \leqslant i \leqslant \alpha, t \in [0, t_i] \tag{7}$$

where $\boldsymbol{T_{ev}}$ represents the extreme-value variable of all the LSFs for each probability space in PDEM. Subsequently, the reliability of the extreme-value event incorporating the influence of several limit states can be obtained as Eq. 8, in which $p_{\boldsymbol{T_{ev}}}$ denotes the extreme value distribution at the virtual time $t = 1$:

$$R = F_{\boldsymbol{T_{ev}}}(\boldsymbol{T_{ev}} > 0,\ t = 1) = \int_0^{\infty} p_{\boldsymbol{T_{ev}}}(\boldsymbol{T_{ev}},\ t = 1) \cdot d\boldsymbol{T_{ev}} \tag{8}$$

2.2. Enhanced framework considering multiple limit states and failure modes

With the Eq. 5, the system reliability analysis can then be introduced. If a system physical object $\boldsymbol{Z(\Theta)}$ is defined as $\boldsymbol{Z_S}(\boldsymbol{\Theta}) - \boldsymbol{Z_R}(\boldsymbol{\Theta})$, where $\boldsymbol{Z_S}(\boldsymbol{\Theta})$ and $\boldsymbol{Z_R}(\boldsymbol{\Theta})$ represent the system response and resistance under the stochastic system vector $\boldsymbol{\Theta}$, respectively, then the reliability of the integrated system can be defined by the event $\{\boldsymbol{Z}(\boldsymbol{\Theta}) < 0\}$. Herein $\boldsymbol{Z}(\boldsymbol{\Theta})$ also reflects the limit state function in the reliability field, as shown in Eq. 9.

$$\boldsymbol{Z(\Theta)} = \boldsymbol{Z_S}(\boldsymbol{\Theta}) - \boldsymbol{Z_R}(\boldsymbol{\Theta}) < 0 \tag{9}$$

Eq. 9 can be further converted into Eq. 10, as both the $\boldsymbol{Z_S}(\boldsymbol{\Theta})$ and $\boldsymbol{Z_R}(\boldsymbol{\Theta})$ are the non-negative numbers.

$$\boldsymbol{Z'}(\boldsymbol{\Theta}) = \boldsymbol{Z}(\boldsymbol{\Theta})/\boldsymbol{Z_R}(\boldsymbol{\Theta}) = \boldsymbol{Z_S}(\boldsymbol{\Theta})/\boldsymbol{Z_R}(\boldsymbol{\Theta}) - 1 < 0 \tag{10}$$

Eq. 10 gives a single limit state function (LSF) characterized by a specific performance index (PI), and this is also the most commonly adopted expression in the reliability analysis. For instance, in the bearing capacity evaluation of reinforced concrete beams or columns, $\boldsymbol{Z_S}(\boldsymbol{\Theta})$ and $\boldsymbol{Z_R}(\boldsymbol{\Theta})$ are commonly defined as the single PI of flexural bearing response and flexural bearing resistance (i.e., flexural failure mode); in the seismic deformation evaluation of reinforced concrete frames, $\boldsymbol{Z_S}(\boldsymbol{\Theta})$ and $\boldsymbol{Z_R}(\boldsymbol{\Theta})$ are commonly defined as the single PI of maximum interstory drift response and maximum interstory drift resistance (i.e., displacement failure mode). However, in the actual engineering analysis, a structural system is macroly determined by multiple PIs and multiple failure modes. For the aforementioned beams or columns, the shear failure mode is also a critical parameter, thus the shear bearing response / resistance and multiple failure modes of components may give a more comprehensive assessment; for the aforementioned frames, the floor acceleration failure mode is also a critical parameter, thus the floor acceleration response / resistance and multiple failure modes of frames may give a more comprehensive assessment. In light of this requirement, the multi-limit states and multi-failure modes are introduced for reliability analysis, and Eq. 10 can be converted to Eq. 11:

$$\boldsymbol{Z'}(\boldsymbol{\Theta}) = g[\boldsymbol{Z_{Si}}(\boldsymbol{\Theta}),\ \boldsymbol{Z_{Ri}}(\boldsymbol{\Theta})] - 1 < 0 \tag{11}$$

where $g[\cdot]$ is the function of $\boldsymbol{Z_{Si}}(\boldsymbol{\Theta})$ and $\boldsymbol{Z_{Ri}}(\boldsymbol{\Theta})$, considering multiple limit states and failure modes, and herein i denotes the ith PI and ith corresponding failure mode. In this paper, we give two specific forms of $g(\cdot)$ with physical meanings, i.e., $g1[\boldsymbol{Z_{Si}}(\boldsymbol{\Theta}),\ \boldsymbol{Z_{Ri}}(\boldsymbol{\Theta})]$ and $g2[\boldsymbol{Z_{Si}}(\boldsymbol{\Theta}),\ \boldsymbol{Z_{Ri}}(\boldsymbol{\Theta})]$, as presented in Eqs. 12 and 13.

$$\boldsymbol{Z1'}(\boldsymbol{\Theta}) = g1[\boldsymbol{Z_{Si}}(\boldsymbol{\Theta}),\ \boldsymbol{Z_{Ri}}(\boldsymbol{\Theta})] - 1 = \sum_{i=1}^{\alpha}[\boldsymbol{Z_{Si}}(\boldsymbol{\Theta})/\boldsymbol{Z_{Ri}}(\boldsymbol{\Theta})]^{q_i} - 1 < 0 \tag{12}$$

$$\begin{aligned} \boldsymbol{Z2'}(\boldsymbol{\Theta}) &= g2[\boldsymbol{Z_{Si}}(\boldsymbol{\Theta}),\ \boldsymbol{Z_{Ri}}(\boldsymbol{\Theta})] - 1 \\ &= max\left\{\boldsymbol{Z_{S1}}(\boldsymbol{\Theta})/\boldsymbol{Z_{R1}}(\boldsymbol{\Theta}),\ ...,\ \boldsymbol{Z_{Si}}(\boldsymbol{\Theta})/\boldsymbol{Z_{Ri}}(\boldsymbol{\Theta}),\ ...,\ \boldsymbol{Z_{S\alpha}}(\boldsymbol{\Theta})/\boldsymbol{Z_{R\alpha}}(\boldsymbol{\Theta})\right\} - 1 < 0 \end{aligned} \tag{13}$$

where α represents the number of multi-failure modes considered in the analysis. Figs. 1(a) and 1(b) present the physical meanings of Eqs. 12 and 13, when the multiple limit states are adopted as 2 and 3, respectively. As for Eq. 12, when the q_i is constant as 1 or 2, the corresponding physical meanings of multi-LSFs respond to the circle combination (i.e., combination 1) and triangle combination (i.e., combination 2) in Fig. 1, respectively. As for Eq. 13, the corresponding physical meanings of multi-LSFs respond to the square combination (i.e., combination 3) in Fig. 1.

As both the $\boldsymbol{Z1'}(\boldsymbol{\Theta})$ and $\boldsymbol{Z2'}(\boldsymbol{\Theta})$ only depend on the $\boldsymbol{\Theta}$, thus $\boldsymbol{Z1'}(\boldsymbol{\Theta})$ and $\boldsymbol{Z2'}(\boldsymbol{\Theta})$ can also be regarded as the concerned physical object in PDEM, and during the analysis, the equivalent extreme-value event is required for analysis as mentioned before. Thus, replace the $\boldsymbol{H}(\boldsymbol{\Theta}, t)$ in Eq. 2 with $\boldsymbol{Z'}(\boldsymbol{\Theta}, t)$, and establish the virtual stochastic process. For each point set $\boldsymbol{\Theta}_i$, the deterministic dynamic or static analyses are conducted to obtain the derivative of the concerned physical variable, i.e., $\dot{\boldsymbol{Z}}'(\boldsymbol{\Theta}_i, t)$, and the value is brought into Eq. 2

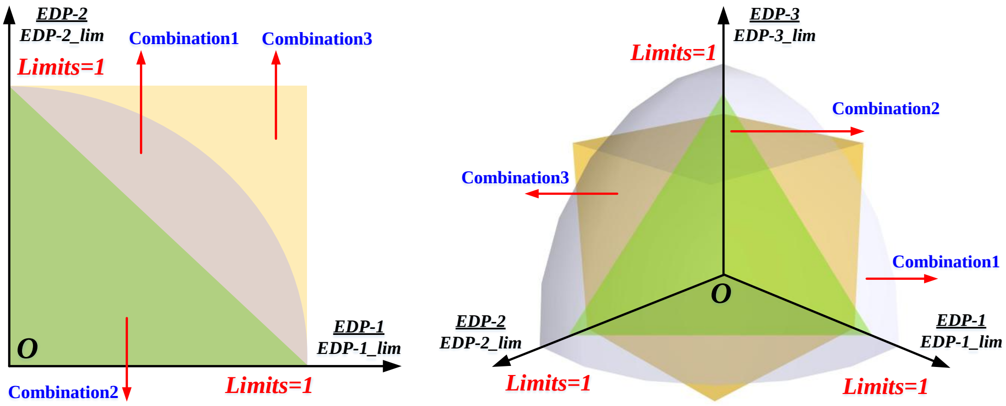

(a) Two dimensional conditions

(b) Three dimensional conditions

Figure 1: The physical meanings of multi-LSFs and multi-failure modes considered in the enhanced PDEM

to realize the discretization of GDEE, as denoted in Eq. 14:

$$\frac{\partial p_{\boldsymbol{Z'}\boldsymbol{\Theta}}(\boldsymbol{Z'},\ \boldsymbol{\Theta},\ t)}{\partial t} + \dot{\boldsymbol{Z}}'(\boldsymbol{\Theta}, t) \cdot \frac{\partial p_{\boldsymbol{Z'}\boldsymbol{\Theta}}(\boldsymbol{Z'},\ \boldsymbol{\Theta},\ t)}{\partial \boldsymbol{Z'}} = 0 \tag{14}$$

The GDEE can be solved via finite difference methods to obtain the PDF of the concerned physical object, $\boldsymbol{Z'}(t)$, as mentioned in Eq. 15, where m denotes the number of representative point sets with different probability-assigned space. As for the equivalent extreme-value event, we chose the evaluation results at the virtual time of t=1. Afterwards, the system reliability (R) can then be assessed by Eq. 16, at the boundary condition of $\boldsymbol{Z'}$=0.

$$p_{\boldsymbol{Z'}}(\boldsymbol{Z'},\ t=1) = \sum_{i=1}^{m} p_{\boldsymbol{Z'}\boldsymbol{\Theta}}(\boldsymbol{Z'},\ \boldsymbol{\Theta}_i,\ t=1) \tag{15}$$

$$R = F_{\boldsymbol{Z'}}(\boldsymbol{Z'} < 0,\ t=1) = \int_{-\infty}^{0} p_{\boldsymbol{Z'}}(\boldsymbol{Z'},\ t=1) \cdot d\boldsymbol{Z'} \tag{16}$$

The PDEM avoids the pre-defined distribution of concerned physical object and obviously reduces the calculation burden. Meanwhile, the combined PI considering multiple limit states is introduced to enhance the PDEM-based framework for reliability analysis, thus a more comprehensive assessment conclusion can be drawn. Fig. 2 presents the detailed schematic steps of the enhanced PDEM framework considering multiple limit states and failure modes.

3. Implementation of the enhanced PDEM-based reliability framework

In this section, two case studies are performed to illustrate the effectiveness of the enhanced PDEM-based framework as well as the necessity to consider multiple limit states. The first is a simply supported beam

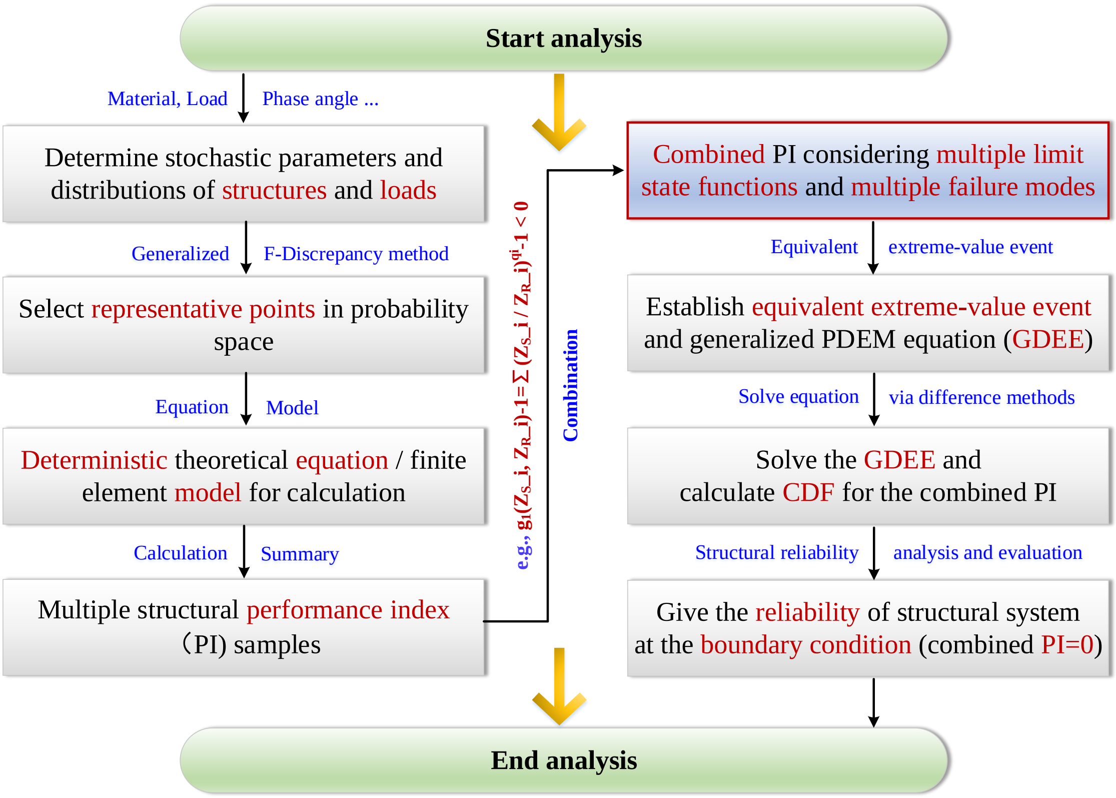

Figure 2: The detailed schematic steps of the enhanced PDEM framework considering multiple limit states and failure modes

under two-point concentrated forces with two failure conditions (i.e., shear failure and flexural failure), and the second is a 3-span-6-story RC frame under seismic excitation with three failure conditions (i.e., maximum displacement failure, residual displacement failure and floor acceleration failure). Meanwhile, the MCS is also performed for both examples as a comparison and validation. The detailed analyses are carried out as follows.

3.1. Case study 1: Simply supported beam with two failure conditions

Fig. 3 presents the dimension information and symbol definition of the adopted simply supported beam in case study 1. Totally 11 random variables are selected, and Tab 1 lists the basic parameters and distributions in case study 1. The section width (b), section height (h), shear length (a) and concentration force (Q) are assumed to conform to normal distributions, and other variables are assumed to conform to lognormal distributions. During the analysis, the tensile strength of concrete (f_t) is taken as 1/10 of the compressive strength (f_c). Under the enhanced PDEM framework, the selection of representative points is the first step, and in this example 300 points with different assigned probability are primarily generated using the optimal minimum F-Discrepancy method [47, 48]. Moreover, two failure modes are adopted into the PDEM-based reliability assessment in this study, which are the flexural failure mode and shear failure mode, and three multi-LSFs (i.e., circle, triangle and square combinations) are incorporated according to Eqs. 12 and 13 for comparison. The theoretical value of the flexural resistance (M_R) and flexural response (M_S) for the simply supported beam can be denoted as Eqs. 17 and 18:

$$M_R = f_y \cdot A_s \cdot (h_0 - \frac{1}{2} \cdot \frac{f_y \cdot A_s}{f_c \cdot b}) \tag{17}$$

$$M_S = Q \cdot a \tag{18}$$

where f_y represents the yielding strength of reinforcement steel, and f_c represents the compressive strength of concrete. A_s represents the summary of sectional areas for the longitudinal reinforcement. h_0 denotes the effective sectional height and can be calculated as $h - a_s$, where a_s represents the concrete cover thickness. Q represents the concentration force and a represents the shear length from the action position to the support. As for the theoretical value of the shear resistance (V_R) and shear response (V_S) for the simply supported beam, equations can be denoted as Eqs. 19 and 20:

$$V_R = 0.7 \cdot f_t \cdot b \cdot h_0 + \frac{f_{yv} \cdot A_{sv} \cdot h_0}{s} \tag{19}$$

$$V_S = Q \tag{20}$$

where f_{yv} denotes the stirrup tensile strength, and s denotes the stirrup spacing. A_{sv} denotes the stirrup sectional areas and can be calculated as $2\pi d_{sv}^2/4$, where the coefficient 2 is for double-limb stirrup in this analysis and d_{sv} represents the sectional diameter of stirrup.

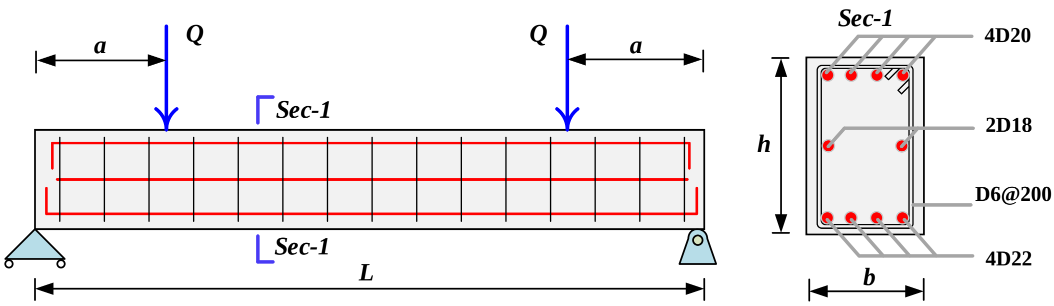

Figure 3: The dimension information and symbol definition of the simply supported beam

Table 1: The stochastic variables and distributions of the simply supported beam

Random variables	*Symbol*	*Distribution*	*Mean*	*COV*
Section width	b	Normal	200 (mm)	0.01
Section height	h	Normal	400 (mm)	0.01
Shear length	a	Normal	750 (mm)	0.01
Concentration force	Q	Normal	110.7 (kN)	0.4
Concrete compressive strength	f_c	Lognormal	15.2 (MPa)	0.1
Rebar tensile strength	fyt	Lognormal	378 (MPa)	0.074
Rebar diameter	dt	Lognormal	25 (mm)	0.04
Rebar elastic modulus	Es	Lognormal	201000 (MPa)	0.033
Stirrup tensile strength	fyv	Lognormal	270 (MPa)	0.074
Stirrup diameter	dsv	Lognormal	6 (mm)	0.04
Stirrup spacing	s	Lognormal	200 (mm)	0.04

Note: Some distribution parameters and values can be referred from [57, 58, 61].

Figs. 4(a) and 4(b) display the CDF, failure probability and reliability of the target variable via PDEM using single LSF and single failure mode (i.e., flexural mode and shear mode, respectively). Worth mentioning is that the result is calculated at the abscissa of 0 according the derivations in Section 2. To be specific, the abscissas are presented as $MS/MR - 1$ and $VS/VR - 1$ for Figs. 4(a) and 4(b), respectively. Through the flexural mode, the acquired failure probability of the simply supported RC beam is 0.0409, and the corresponding reliability is given as 0.9591. In another word, the flexural resistance is generally larger than the flexural response in most stochastic conditions for this simply supported RC beam when analyzed from the aspect of flexure. However, through the shear mode, the acquired failure probability of the simply supported RC beam is 0.544, and the corresponding reliability is given as 0.456. It can be seen that from the aspect of shear failure, the reliability of the simply supported RC beam is sharply lowered compared with the flexural failure. If only single LSF and single failure mode is considered in the reliability assessment, the results obtained are biased and may not be convincing.

Figs. 4(c), 4(d) and 4(e) display the corresponding results via the enhanced PDEM-based framework considering multiple limit states (i.e., circle combination, triangle combination and square combination, respectively). The corresponding abscissas for the three conditions are presented as $(MS/MR)^2 + (VS/VR)^2 - 1$, $MS/MR + VS/VR - 1$ and $max(MS/MR, VS/VR) - 1$ from Figs. 4(c) to 4(e). Generally, two conclusions can be observed. The first conclusion is that after incorporating multiple limit states into the PDEM, the obtained results are more conservative and the calculated reliability is commonly lower than the single condition. The failure probability for the circle, triangle and square combination is shown as 0.6254, 0.8144 and 0.544, respectively, and the acquired reliability for the three combinations is presented as 0.3746, 0.1856 and 0.456, respectively. Compared with the single flexural mode (Fig. 4(a)), the dropping percentage of reliability is 60.9%, 80.6% and 52.5%, and compared with the single shear mode (Fig. 4(b)), the dropping percentage ranges from 17.9% to 59.3%. The second conclusion is that with different combination ways of multiple failure modes and limit states, the obtained reliability presents variation within a certain range. The triangle combination indicates the least reliability compared with the other two combinations, accompanied with the gap ratios of 50.4% and 59.3%. The square combination shows the largest reliability (0.456), and its result equals to the single shear condition in this example, as illustrated in Figs. 4(b) and 4(e). To verify the effectiveness and accuracy of the enhanced PDEM-based framework in reliability assessment considering multiple limit states, MCS is also performed as a comparison, which is commonly adopted as a benchmark approach for crosscheck. The more samples are stochastically generated, the more accurate results can be given. The reliability via MCS (R_{MCS}) can be expressed as Eq. 21:

$$R_{MCS} = \frac{n_s}{N_{tol}} \tag{21}$$

where n_s denotes the reliable point number within the limitations, and N_{tol} denotes the total point number generated in MCS. In this analysis, 10000 points for all the 11 random variables are sampled with the same assigned probability (i.e., 0.0001), and Fig. 5 displays the scattered points of stochastic results in MCS. The black dotted lines represent the single LSF, while the blue, red, and pink solid lines represent the multi-LSFs for a schematic view. Tab 2 lists the data comparison between PDEM and MCS under different LSF types and failure modes in case study 1. It can be found that the calculated results by MCS are generally in consistent with the PDEM. For all the five LSFs listed in Tab 2, the corresponding reliability via MCS is shown as 0.9575, 0.4496, 0.3665, 0.1793 and 0.4496, respectively, and the deviations from PDEM are given as 0.17%, 1.42%, 2.21%, 3.51% and 1.42%, respectively. Meanwhile, the reliability obtained by

MCS that incorporates multiple limit states indicates the same tendency as PDEM (i.e., more conservative with a lower value in comparison with single LSF). In summary, the analyses validate the effectiveness and accuracy of the enhanced PDEM framework for reliability assessment under the consideration of multiple limit states and failure modes. Moreover, the calculating efficiency is obviously improved, as only 300 points are generated in PDEM while 10000 points are generated in MCS.

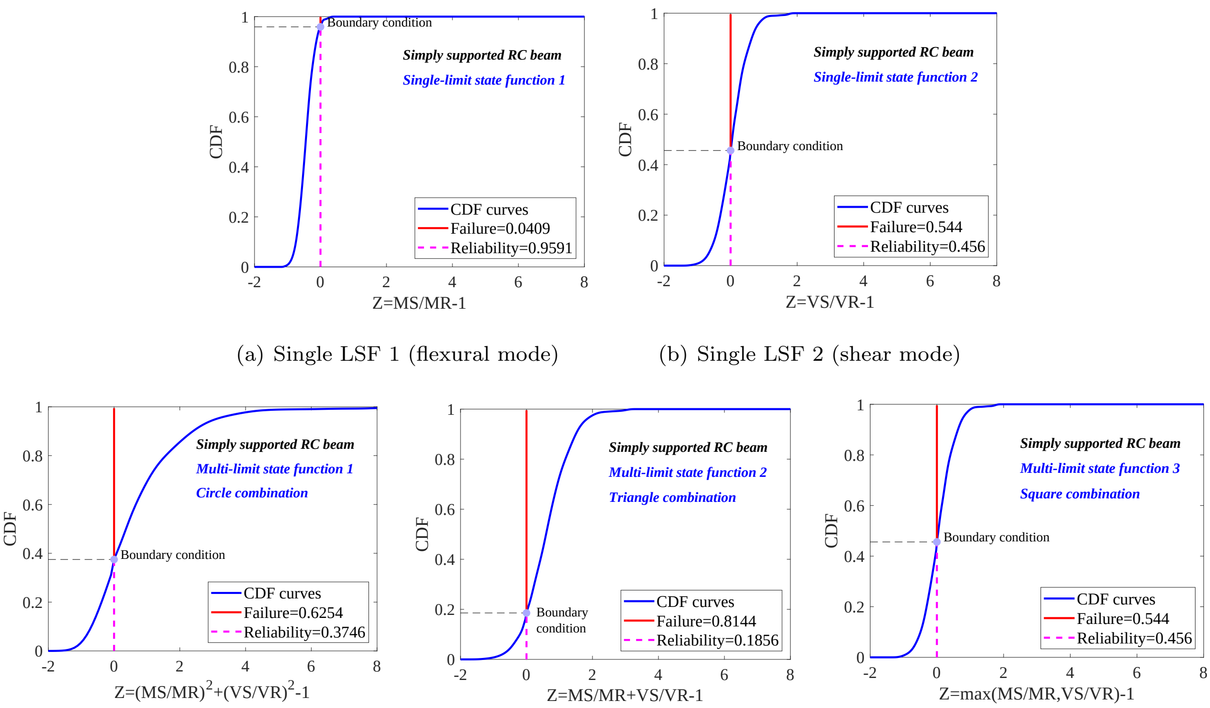

(a) Single LSF 1 (flexural mode) (b) Single LSF 2 (shear mode)

(c) Multi-LSF 1 (circle combination) (d) Multi-LSF 2 (triangle combination) (e) Multi-LSF 3 (square combination)

Figure 4: The CDF, failure probability and reliability of the target variable under different LSFs via PDEM (case study 1)

Table 2: The comparison between PDEM and MCS under different LSF types and failure modes (case study 1)

LSF type and failure mode	***PDEM***		***MCS***		***Deviation***
	Failure	Reliability	Failure	Reliability	(%)
Single LSF 1 (M)	0.0409	0.9591	0.0425	0.9575	0.17
Single LSF 2 (V)	0.5440	0.4560	0.5504	0.4496	1.42
Multi-LSF 1 (M+V circle)	0.6254	0.3746	0.6335	0.3665	2.21
Multi-LSF 2 (M+V triangle)	0.8144	0.1856	0.8207	0.1793	3.51
Multi-LSF 3 (M+V square)	0.5440	0.4560	0.5504	0.4496	1.42

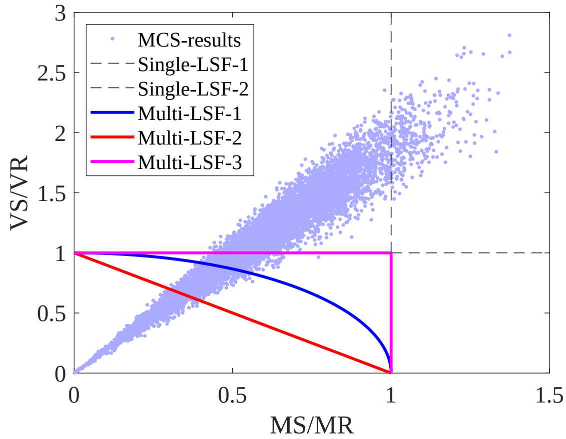

Figure 5: The scattered points and the schematic view of different LSFs via Monte Carlo simulation (10000 points in case study 1)

3.2. Case study 2: Reinforced concrete frame with three failure conditions

Fig. 6(a) presents the dimension information of the adopted RC frame in case study 2, which is excited with the non-stationary stochastic ground motions. Totally 13 random variables are selected, and Tab 3 lists the basic parameters and distributions in case study 2. During the analysis, the non-stationary stochastic earthquake model via the spectrum representation approach is adopted, aiming to reflect the real stochastic scenarios of earthquake input in the practical engineering [62, 63, 64]. The specific generating equations of the non-stationary stochastic earthquake model are not elaborated in this paper and can be available in Liu et al. [65, 66]. The stochastic motion parameters ($\Theta 1$ and $\Theta 2$) are assumed to conform to the uniform distributions and reflect the uncertainty from the earthquake input. The concrete bulk density (γ), beam span (sb), first storey height (hf), standard storey height (ha), rebar diameters ($d20$ and $d25$), damping ratio (ς) are assumed to conform to normal distributions, while the core concrete compressive strength ($f_{cp,core}$), core concrete ultimate strain ($\varepsilon_{cu,core}$), rebar yielding strength (f_y), rebar elastic modulus (E) are assumed to conform to lognormal distributions. The above-mentioned random variables reflect the uncertainty from the structural itself (e.g., material uncertainty and dimension uncertainty). Under the enhanced PDEM framework, the selection of representative points is the first step, and in this example 200 points with different assigned probability are primarily generated using the aforementioned selecting method [47, 48]. Moreover, three failure modes are adopted into the PDEM-based reliability assessment in this study, which are the maximum inter-story drift ratio (MIDR) failure, residual inter-story drift ratio (RIDR) failure, and peak floor acceleration (PFA) failure. Besides, three multi-LSFs (i.e., circle, triangle and square combinations) are also incorporated into the enhanced PDEM-based framework according to Eqs. 12 and 13 for comparison. Worth mentioning is that the benchmark RC frame is assumed to locate at the region with fortification level of 8 degree in China, and the corresponding rare earthquake intensity is adopted as 0.4 g for excitation in this paper (i.e., the exceeding probability of 2% in 50 years). The immediate occupancy performance level is chosen for analysis according to FEMA-356 [67] and HAZUS-MH [68], and the corresponding resistance thresholds for MIDR failure, RIDR failure and PFA failure are determined as 0.01, 0.001, and 0.4 (g), respectively [69].

To carry out the assessment in this example, the OpenSees software is adopted for model establishment, which is a commonly-used tool for simulating the response of structural and geotechnical systems subjected to earthquakes and other hazards [70, 71]. In comparison with the three-dimensional solid models, the OpenSees software reduces the computational cost and simultaneously keeps the nonlinear characteristics [72, 73]. In this modelling, the force-based beam-column elements with fiber cross sections are selected to model the frame beams and columns [74, 75], and five integrations points are defined for each beam-column element. The joint2D element is selected to capture the behaviors of beam-column connections, which contains five springs to characterize the flexural-rotation properties in the core zones. The central spring reflects the shear behavior of the connection panel, while other four springs are located at the beam-column interfaces to reflect the reinforcement bond-slip behaviors. The central spring is assigned with the Pinching4 material in this modelling that can reflect the stiffness degradation and hysteresis pinching, and the four main points in the skeleton curve of Pinching4 material can be obtained in light of the modified compression field theory. The other four springs are assigned with the Hysteretic material in this modelling, and the corresponding characteristic points can be calculated after introducing a unit-length fiber section analysis and zero-length section element. The EqualDOF constraint is adopted to limit the horizontal displacement for each floor, based on the rigid floor assumption. Fig. 6(b) displays the simulation model and element assignment of the 3-span-6-story RC frame in this example. A comparison with the experimentally hysteretic data in reference [76] is also presented in Fig. 6(b), which verifies the effectiveness and appropriateness of the established model for the subsequent reliability assessment in a sense. With related to the details of modelling strategy, more references can be found in Feng et al. [77, 78] and Cao et al. [79, 80, 81].

Figs. 7(a), 7(b) and 7(c) display the CDF, failure probability and reliability of the target variable via PDEM using single LSF and single failure mode (i.e., MIDR failure mode, RIDR failure mode and PFA failure mode, respectively). Worth mentioning is that the result is calculated at the abscissa of 0 according the derivations in Section 2. The abscissas are presented as $\theta S/\theta R-1$, $\theta rS/\theta rR-1$ and $FaS/FaR-1$ from Figs. 7(a) to 7(c), respectively. Through the MIDR failure mode, the acquired failure probability of the adopted RC frame is 0.3077, and the corresponding reliability is given as 0.6923. Through the RIDR failure mode, the acquired failure probability of the adopted RC frame is 0.1537, and the corresponding reliability is given as 0.8463. Through the PFA failure mode, the acquired failure probability of the adopted RC frame is 0.2407, and the corresponding reliability is given as 0.7593. As for the single LSF, the calculated reliability is largely dependent on the selected failure mode, and the gap percentage among the results can be as high as 15.4% in this example. In another word, if only single LSF and single failure mode is adopted, say, the

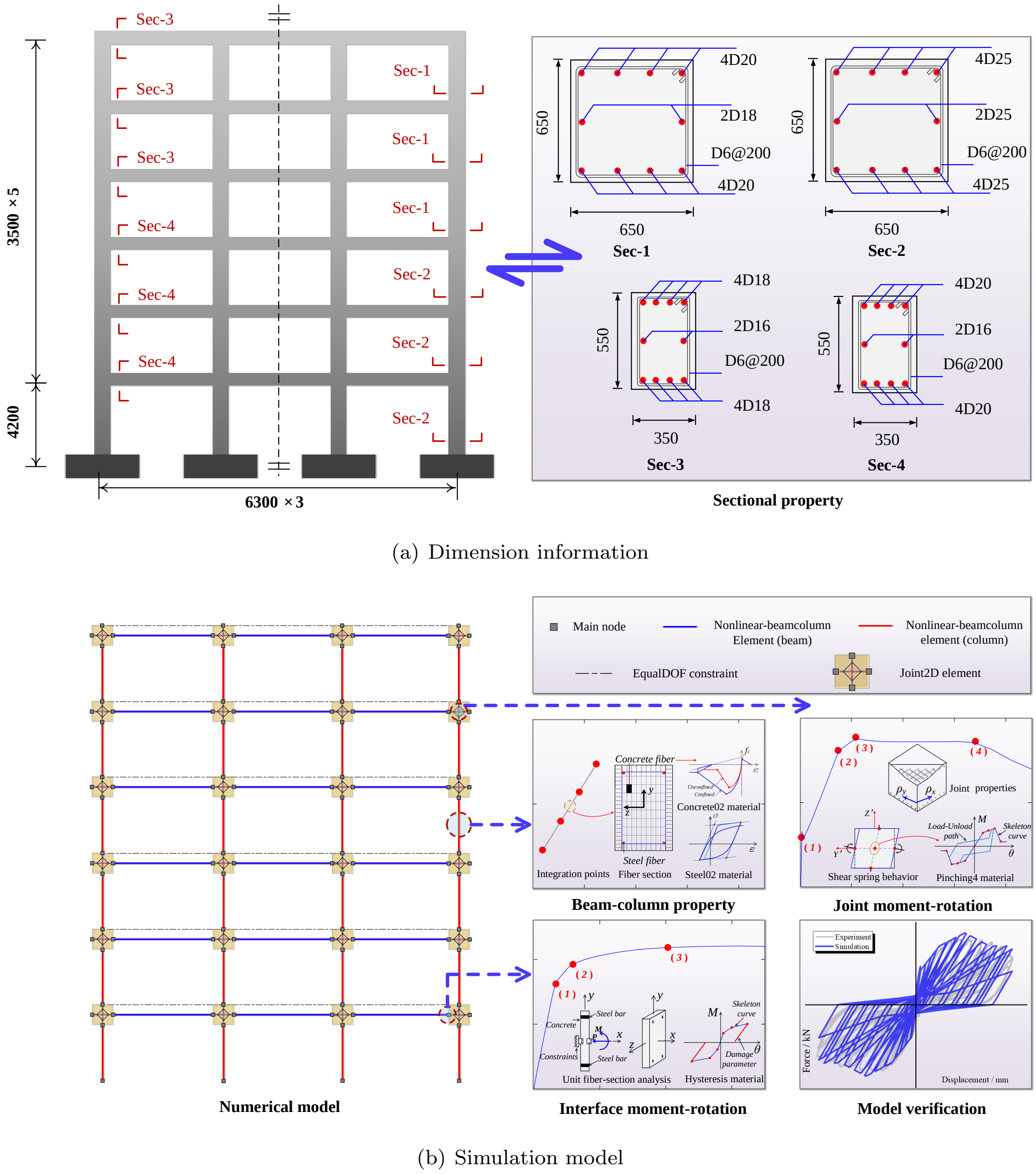

Figure 6: The dimension information and simulation model of the RC frame

Table 3: The stochastic variables and distributions of the RC frame

Random variables	***Symbol***	***Distribution***	***Mean***	***COV***
Stochastic motion parameter	$\Theta 1$	Uniform	3.142 (1)	0.577
Stochastic motion parameter	$\Theta 2$	Uniform	3.142 (1)	0.577
Concrete bulk density	γ	Normal	26.5 (kN/m^3)	0.0698
Beam span	sb	Normal	6300 (mm)	0.003
First storey height	hf	Normal	4200 (mm)	0.003
Standard storey height	ha	Normal	3500 (mm)	0.003
Core concrete compressive strength	$f_{cp,core}$	Lognormal	33.6 (MPa)	0.21
Core concrete ultimate strain	$\varepsilon_{cu,core}$	Lognormal	0.0113 (1)	0.52
Rebar diameter in columns	$d25$	Normal	25 (mm)	0.04
Rebar diameter in beams	$d20$	Normal	20 (mm)	0.04
Rebar yielding strength	f_y	Lognormal	378 (MPa)	0.074
Rebar elastic modulus	E	Lognormal	201000 (MPa)	0.033
Damping ratio	ς	Normal	0.05 (1)	0.1

Note: Some distribution parameters and values can be referred from [57, 82, 83, 84].

commonly-used MIDR with the reliability of 0.6923, the calculating result is much conservative and there exists certain controversy especially when compared with the other two failure patterns, i.e., RIDR mode (0.8463) and PFA mode (0.7593). The comparison further illustrates the significance of considering multiple limit states and failure modes in the structural reliability evaluation.

Figs. 7(d), 7(e) and 7(f) display the corresponding results via the enhanced PDEM-based framework considering multiple limit states (i.e., circle combination, triangle combination and square combination, respectively). The corresponding abscissas for the three conditions are presented as $(\theta S/\theta R)^2+(\theta rS/\theta rR)^2+(FaS/FaR)^2-1$, $\theta S/\theta R+\theta rS/\theta rR+FaS/FaR-1$ and $max(\theta S/\theta R, \theta rS/\theta rR, FaS/FaR)-1$ from Figs. 7(d) to 7(f). It can be found that after incorporating multiple limit states and failure modes into the PDEM, the obtained results are more conservative and the calculated reliability is commonly lower than the single condition. The failure probability for the circle, triangle and square combination is shown as 0.9159, 0.9672 and 0.4847, respectively, and the acquired reliability for the three combinations is presented as 0.0841, 0.0328 and 0.5153, respectively. Compared with the single MIDR failure mode (Fig. 7(a)), the dropping percentage of reliability is 87.9%, 95.3% and 25.6%, and compared with the single RIDR failure mode (Fig. 7(b)), the dropping percentage ranges from 39.1% to 96.1%. As for the single PFA failure mode in Fig. 7(c), the reliability deviations for the three combinations vary from 32.1% to 95.7%, also indicating a large extent. The obvious drop in reliability in Figs. 7(d) and 7(e) mainly results from the three failure modes selected as a criterion in this example, and multiple limit states significantly raise the threshold for the reliability requirement. Take the square combination in Fig. 7(f) as an example, which is the most intuitive way. The square combination uses the maximum value among all the single failure modes as the PDEM sample, and the corresponding reliability presents the decreasing extent of 0.177 (25.6%), 0.331 (39.1%), and 0.244 (32.1%), respectively. In a sense, after incorporating multiple limit states and failure modes, the obtained result can be more convincing and comprehensive.

To verify the effectiveness and accuracy of the enhanced PDEM-based framework in reliability assessment considering multiple limit states and failure modes, MCS is also performed as a comparison. In this analysis, 10000 points for all the 13 random variables are sampled with the same assigned probability (i.e., 0.0001), and Fig. 8 presents the scattered points of stochastic results in MCS. Figs. 8(a) and 8(d) display the views of circle combination for multi-LSF 1, Figs. 8(b) and 8(e) display the views of triangle combination for multi-LSF 2, and Figs. 8(c) and 8(f) display the views of square combination for multi-LSF 3. Tab 4 lists the data comparison between PDEM and MCS under different LSF types and failure modes in case study 2. It can be observed that the calculated results by MCS are generally in consistent with the PDEM. For all the six LSFs listed in Tab 4, the failure probability given by MCS is displayed as 0.3206, 0.1427, 0.2791, 0.9093, 0.9692 and 0.4937. The corresponding reliability via MCS is shown as 0.6794, 0.8573, 0.7209, 0.0907, 0.0308 and 0.5063, respectively, and the deviations from PDEM are given as 1.90%, 1.28%, 5.33%, 7.28%, 6.49% and 1.78%, respectively. Confronted with the single LSF and failure pattern, the reliability via MCS after considering multiple limit states and different destruction conditions is also more conservative with a lower value, as demonstrated in the results from the enhanced PDEM procedure. The analyses between the MCS and PDEM also prove the accuracy of the enhanced PDEM framework, and for all the LSFs little difference is observed with the maximum deviation of 7.28%. At the same time, in this example, only 200 points are required for the enhanced PDEM-based reliability assessment while 10000 points are required for the MCS-based reliability assessment, signifying the great efficiency improvement in calculation via PDEM.

Table 4: The comparison between PDEM and MCS under different LSF types and failure modes (case study 2)

LSF type and failure mode	***PDEM***		***MCS***		***Deviation***
	Failure	Reliability	Failure	Reliability	(%)
Single LSF 1 (MIDR)	0.3077	0.6923	0.3206	0.6794	1.90
Single LSF 2 (RIDR)	0.1537	0.8463	0.1427	0.8573	1.28
Single LSF 3 (PFA)	0.2407	0.7593	0.2791	0.7209	5.33
Multi-LSF 1 (MIDR+RIDR+PFA circle)	0.9159	0.0841	0.9093	0.0907	7.28
Multi-LSF 2 (MIDR+RIDR+PFA triangle)	0.9672	0.0328	0.9692	0.0308	6.49
Multi-LSF 3 (MIDR+RIDR+PFA square)	0.4847	0.5153	0.4937	0.5063	1.78

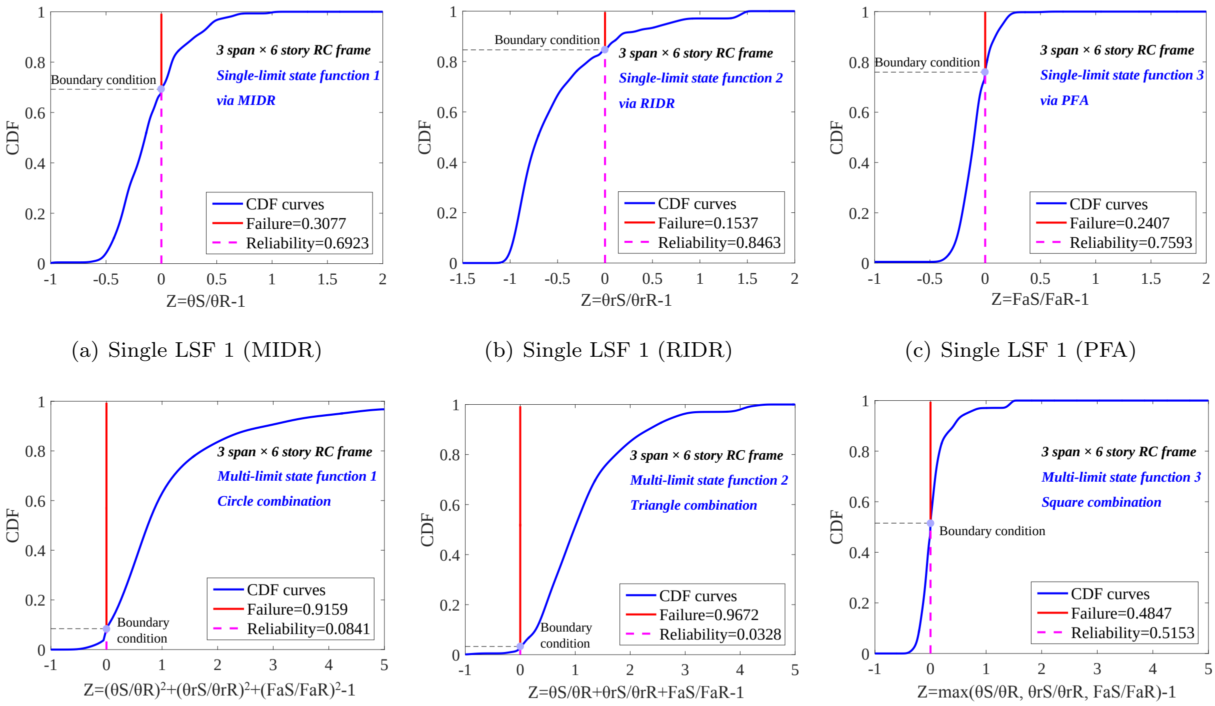

(a) Single LSF 1 (MIDR) (b) Single LSF 1 (RIDR) (c) Single LSF 1 (PFA)

(d) Multi-LSF 1 (circle combination) (e) Multi-LSF 2 (triangle combination) (f) Multi-LSF 3 (square combination)

Figure 7: The CDF, failure probability and reliability of the target variable under different LSFs via PDEM (case study 2)

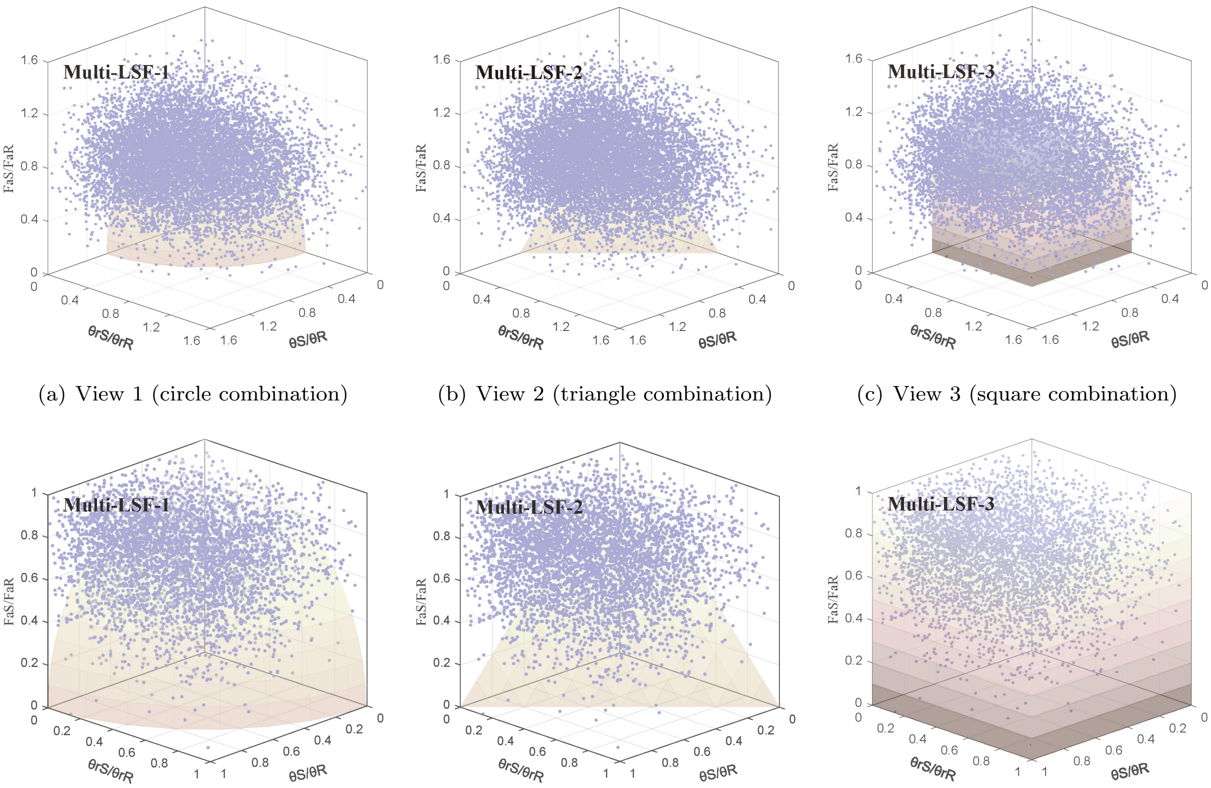

(a) View 1 (circle combination) (b) View 2 (triangle combination) (c) View 3 (square combination)

(d) View 4 (circle combination) (e) View 5 (triangle combination) (f) View 6 (square combination)

Figure 8: The scattered points and the schematic view of different LSFs via Monte Carlo simulation (10000 points in case study 2)

4. Parametric studies in the enhanced PDEM-based reliability framework

In this section, parametric studies pertaining to two significant aspects in the enhanced PDEM-based framework are primarily performed for illustration [85, 86, 87], including a modified equation of the target variable value via representative points incorporating the influence of individual quantile parameters (e.g., 16%, 50% and 84% quantile), as well as the other potential combination types in the enhanced PDEM-based framework (i.e., more than circle, triangle, square ways). The detailed illustrations are shown as follows.

4.1. Modified equation considering individual quantile parameters

As mentioned above, the first step in the enhanced PDEM framework for reliability assessment is to determine the representative points, and the properties of the selected points will directly decide the CDF tendency as well as the calculated reliability. In this subsection, we propose a modified equation of the target physical variable value of representative points, and during the process the selected benchmark points are required for modification, as expressed in Eq. 22:

$$L_{j-mod} = L_j - (L_j - L_{ben-j}) \cdot \frac{|L_j - L_{ben-j}|}{\sum_{i=1}^{\alpha} |L_i - L_{ben-i}|}, \quad j = 1, 2, ..., \alpha \tag{22}$$

where α represents the number of multi-failure modes considered in the analysis. L_j, L_{j-ben} and L_{j-mod} represent the initial target variable value (before modification), the benchmark variable value, and the modified target variable value (after modification), respectively, under the condition of jth failure mode. Worth mentioning is that all the L_j, L_{j-ben} and L_{j-mod} herein are expressed as the response divided by the resistance in calculation for all the failure modes (i.e., S/R), and the modified results of the physical variables are further taken into Eqs. 12 and 13 for the enhanced PDEM-based reliability assessment. Worth noticing is that the symbol L in Eq. 22 is in vector form, i.e., if the representative point number is 200, the above-mentioned modified equation is used for all the 200 samples under each failure pattern. Fig. 9 displays the schematic view of the modified procedure of the target physical variable value in PDEM, based on the multi-LSF 1 (i.e., circle combination). The points A, B and C denote the benchmark point, stochastic point before modification and stochastic point after modification. The distances a, b and c are the embodied representation of $|L_j - L_{ben-j}|$ in Eq. 22. Figs. 9(a) and 9(b) present the two dimensional conditions and three dimensional conditions, respectively.

According to Eq. 22, the selection of benchmark variable value L_{j-ben} influences the modified procedure as well as the reliability assessment. In this subsection, we adopt the quantile parameters of the individual variable in the single LSF and single failure mode as the benchmark for an example. Three quantile levels are used, which are 16%, 50% and 84% quantile, respectively. Fig. 10 presents the modified CDF, failure probability and reliability of the target variable via PDEM and multi-LSF 3. Figs. 10(a) to 10(c) display the modified results in case study 1, and Figs. 10(d) to 10(f) display the modified results in case study 2.

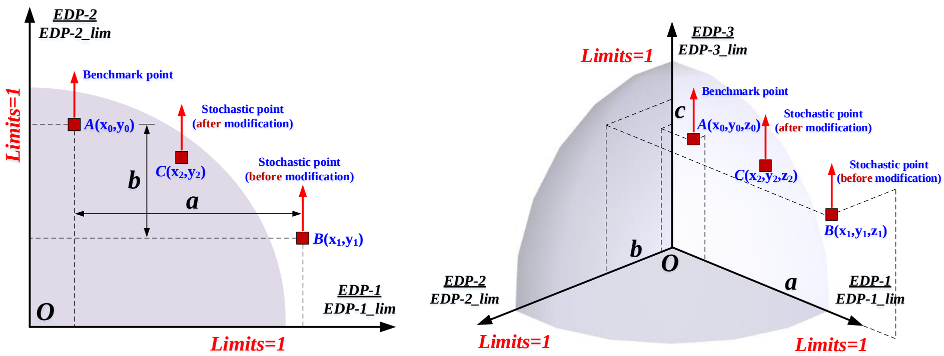

(a) Two dimensional conditions

(b) Three dimensional conditions

Figure 9: The schematic view of the modified procedure of the target physical variable value in PDEM

It can be observed that the reliability via multi-LSF 3 in case study 1 before modification is given as 0.456, while the results after modification come to 0.6228, 0.3682 and 0.1326 for the 16%, 50% and 84% quantile, respectively. The reliability variation ranges from 0.0878 to 0.3234. As for case study 2, the reliability via multi-LSF 3 before modification is given as 0.5153, while the results after modification come to 0.8843, 0.6524 and 0.4628 for the 16%, 50% and 84% quantile, respectively. The corresponding reliability variations are 0.369, 0.1371 and 0.0525 for the three quantile levels, respectively. Generally, the smaller quantile level as the benchmark will increase the reliability result, and the larger quantile level as the benchmark will decrease the reliability result. The detailed comparison of the reliability results before and after modification via the enhanced PDEM framework is summarized in Tab. 5. The modification procedure in this subsection can provide some reference for the future work in the enhanced PDEM-based reliability framework (e.g., benchmark point optimization, quantile level determination).

Table 5: The comparison of the reliability results before and after modification via the enhanced PDEM framework

Quantile level	***Before modification***		***After modification***		***Variation***
	Failure	Reliability	Failure	Reliability	(1)
16% (example 1)	0.544	0.456	0.3772	0.6228	0.1668
50% (example 1)	0.544	0.456	0.6318	0.3682	0.0878
84% (example 1)	0.544	0.456	0.8674	0.1326	0.3234
16% (example 2)	0.4847	0.5153	0.1157	0.8843	0.369
50% (example 2)	0.4847	0.5153	0.3476	0.6524	0.1371
84% (example 2)	0.4847	0.5153	0.5372	0.4628	0.0525

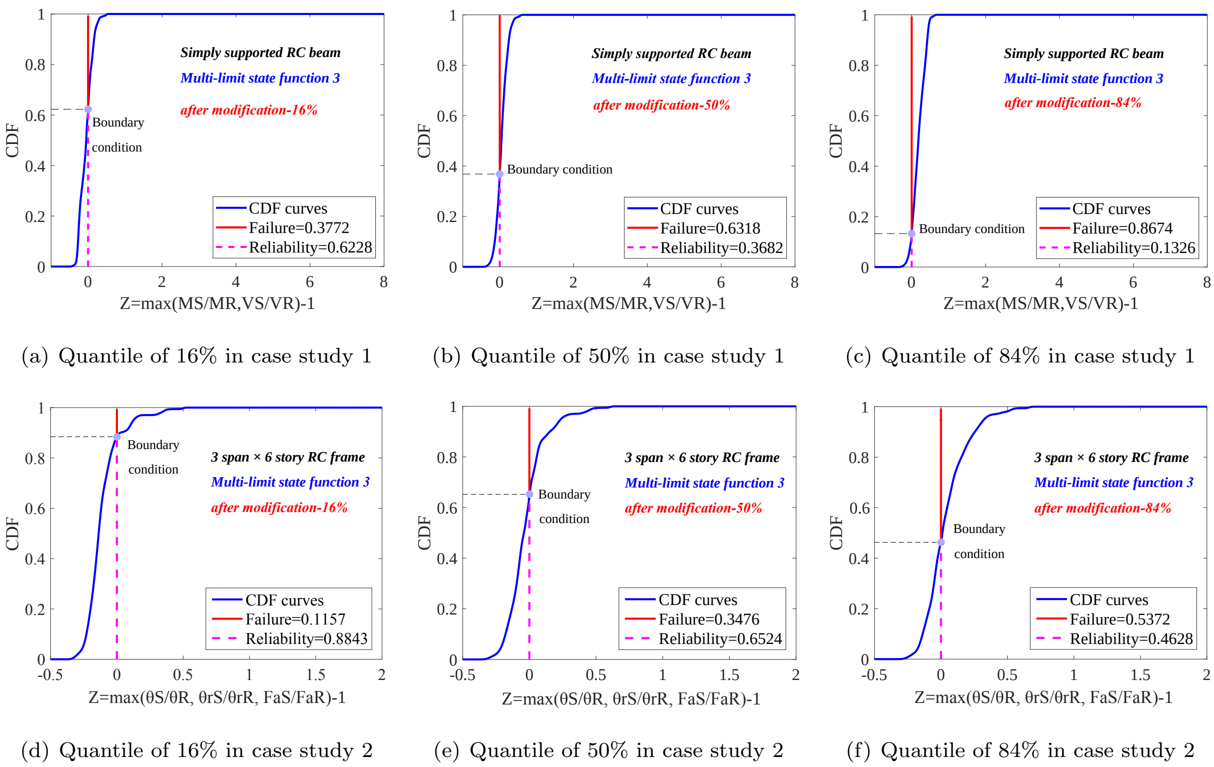

(a) Quantile of 16% in case study 1 (b) Quantile of 50% in case study 1 (c) Quantile of 84% in case study 1

(d) Quantile of 16% in case study 2 (e) Quantile of 50% in case study 2 (f) Quantile of 84% in case study 2

Figure 10: The modified CDF, failure probability and reliability of the target variable via PDEM and multi-LSF 3

4.2. Other combination types considering multiple limit state functions

In the aforementioned analyses, multi-LSFs and failure modes are detailedly discussed in the enhanced PDEM-based reliability framework, and three combination ways (i.e., circle, triangle, and square) are specifically illustrated in light of the Eqs. 12 and 13. In fact, there can also be other combination ways of multiple failure modes in the enhanced PDEM-based reliability framework, and the combination types largely depend on the coefficients in Eqs. 12 and 13 (e.g., q_i). Herein we give some results of other combination ways for illustration. Figs. 11 and 12 present the six other potential combination types incorporating multiple limit states in both case study 1 and 2. The coefficients q_i in Fig. 11 are selected as $\{1, 2\}$, $\{2, 1\}$, $\{1, 3\}$, $\{3, 1\}$, $\{2, 3\}$ and $\{3, 2\}$ for the two adopted failure modes (i.e., flexural mode, shear mode), respectively. For all the six conditions in Fig. 11, the obtained reliability is calculated as 0.2847, 0.3085, 0.3636, 0.3773, 0.4275 and 0.4194. In comparison with the circle combination (q_i=2) with the reliability of 0.3746, the variation ratios are $\{23.9\%, 17.6\%, 2.94\%, 0.72\%, 14.1\%, 11.9\%\}$, while in comparison with the triangle combination (q_i=1) with the reliability of 0.1856, the variation ratios exceed over 53.4%. The changes of coefficient q_i lead to the fluctuation of failure boundary and affect the results of reliability assessment. As for Figs. 12(a) to 12(c), all the coefficients q_i are equally chosen as 1.5, 2.5 and 3. As for Figs. 12(d) to 12(f), the coefficients q_i for the three adopted failure modes (i.e., MIDR mode, RIDR mode, PFA mode) are given as $\{1, 2, 3\}$, $\{2, 1, 3\}$ and $\{3, 2, 1\}$, respectively. For all the six conditions in Fig. 12, the obtained reliability is calculated as 0.0194, 0.1549, 0.2251, 0.0384, 0.0864 and 0.0921. Compared with the reliability via the circle way (0.0841), triangle way (0.0328), and square way (0.5153) as mentioned in Section 3, less changes are found in the former two ways with the range from 0.0023 to 0.1923, while the variations fluctuate from 0.2902 to 0.4959 in the last way. In general, with the increase of the coefficient q_i, the boundary limitation of the whole structural failure is elevated and the system is prone to be more reliable under the same condition (i.e., with a higher reliability).

Fig. 13 presents the schematic view of different LSFs and combination types in case study 1 with two failure modes. The scattered points are the representative points via the enhanced PDEM-based framework, and the other lines indicate the other combination types with different q_1 and q_2. It can be found that with the increase of the coefficient q_i, the envelope range of the corresponding curve is also promoted, and the scattered points that fall within the envelope range enlarge at the same time. Take Fig. 13(a) as an example, the black dotted straight line (q_1=1, q_2=1) represent the triangle combination illustrated in Section 3 and the corresponding reliability is obtained as 0.1856. With the increase of q_1 to 2 and q_2 to 3 (i.e., the solid gray line in Fig. 13(c)), the envelope range is obviously enlarged than the black dotted straight line, and the reliability is also increased with the result of 0.4275, as presented in Fig. 11(e). The obtained result (q_1=2, q_2=3, reliability of 0.4275) is even larger than the circle combination (q_1=2, q_2=2, reliability of 0.3746), which also agrees with the above conclusion. Similar phenomenon can be observed for other combinations, say, the pink dotted line (q_1=3, q_2=2, reliability of 0.4194) and the black dotted line (q_1=3, q_2=1, reliability of 0.3773) in Fig. 13(e).

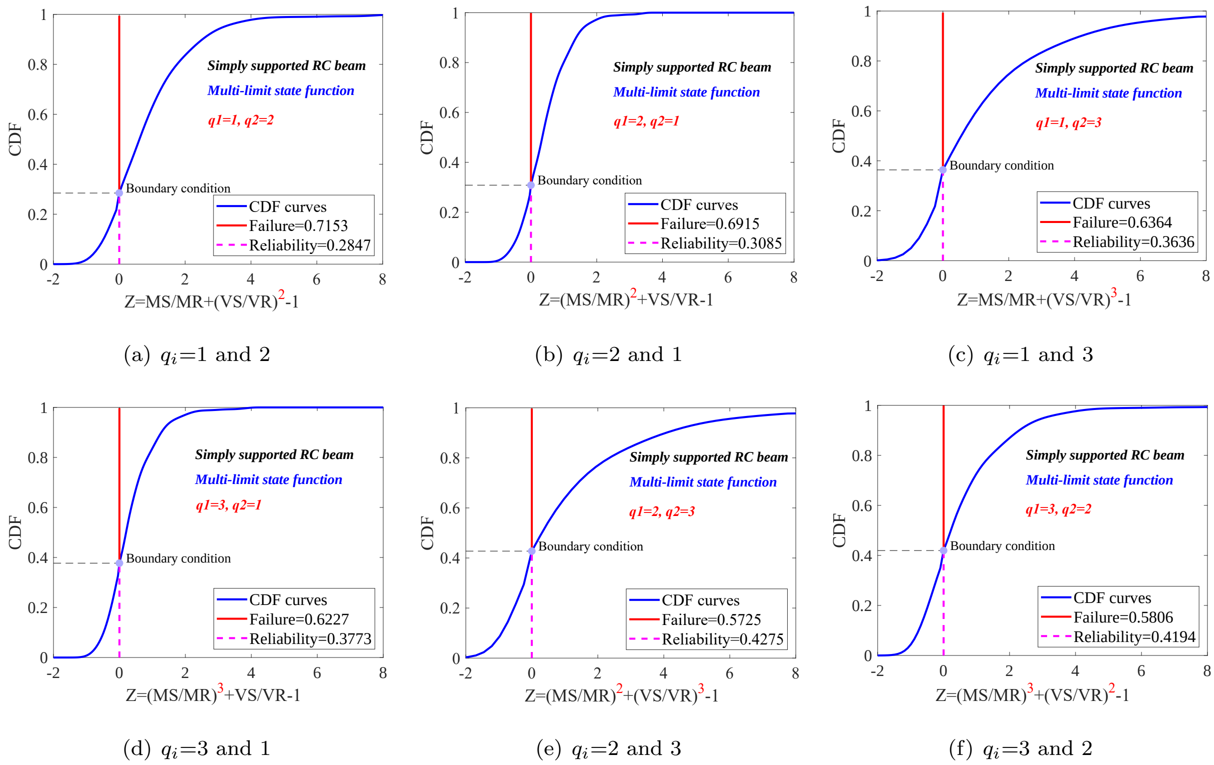

(a) q_i=1 and 2 (b) q_i=2 and 1 (c) q_i=1 and 3

(d) q_i=3 and 1 (e) q_i=2 and 3 (f) q_i=3 and 2

Figure 11: Other combination types considering multiple limit states in case study 1

Another finding is that when q_i is large enough, the obtained result is close to the form of $max(\cdot)$ via Eq. 13 (i.e., square combination). Take Fig. 13(l) for illustration, with the increase of q_1 to 50 and q_2 to 10 (red solid line), the envelope range aggressively approximates to the vertical line $MS/MR = 1$ (i.e., single LSF 1) and the horizontal line $VS/VR = 1$ (i.e., single LSF 2), and the schematic meaning of the square combination is the merge of the two single LSFs, as illustrated in Fig. 5. Fig. 14 displays the schematic view of different LSFs and combination types in case study 2 with three failure modes, among which Figs. 14(d) (q_1=1, q_2=1, q_3=1) and 14(e) (q_1=2, q_2=2, q_3=2) are in consistent with the triangle combination and circle combination in Fig. 8. Worth mentioning is the Fig. 14(j) (q_1=15, q_2=15, q_3=15, quite large), where the envelope range of failure boundary is quite close to the square combination in Fig. 8(c), which also proves the rationality of conclusion as mentioned above. Besides, with the variation of q_i from 0 to 1 (e.g., Figs. 14(a) to 14(c), 14(v) to 14(ad)), the envelope range shrinks in a sense, and the corresponding points that satisfy within the boundary condition are reduced, accompanied with a lower system reliability. In summary, the parametric studies of other combination types that incorporate multiple failure conditions in this subsection shed some light for the development trend and boundary rule of multi-LSF in PDEM, and meanwhile provide some reference for the future work in the enhanced PDEM-based reliability framework (e.g., appropriate

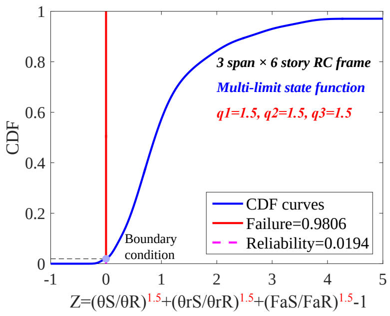

(a) q_i=1.5, 1.5 and 1.5

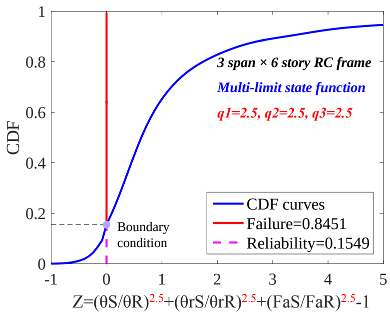

(b) q_i=2.5, 2.5 and 2.5

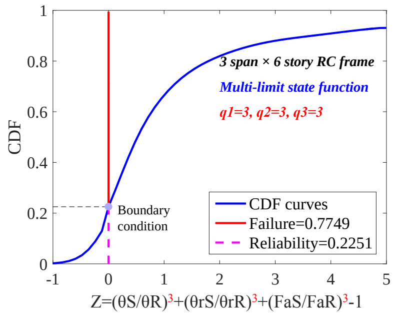

(c) q_i=3, 3 and 3

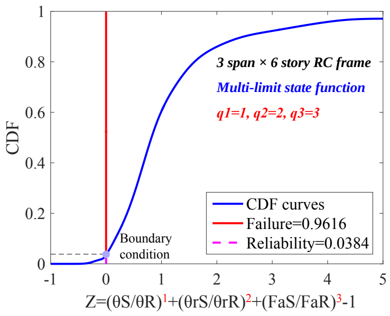

(d) q_i=1, 2 and 3

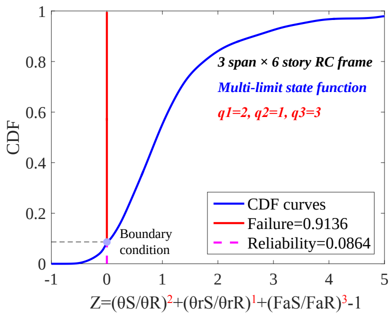

(e) q_i=2, 1 and 3

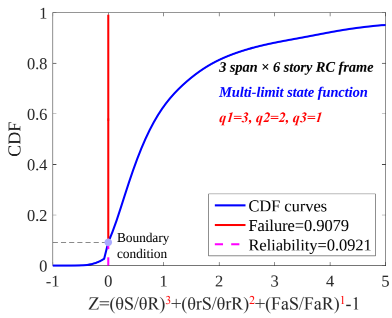

(f) q_i=3, 2 and 1

Figure 12: Other combination types considering multiple limit states in case study 2

combination principle, optimal combination coefficient).

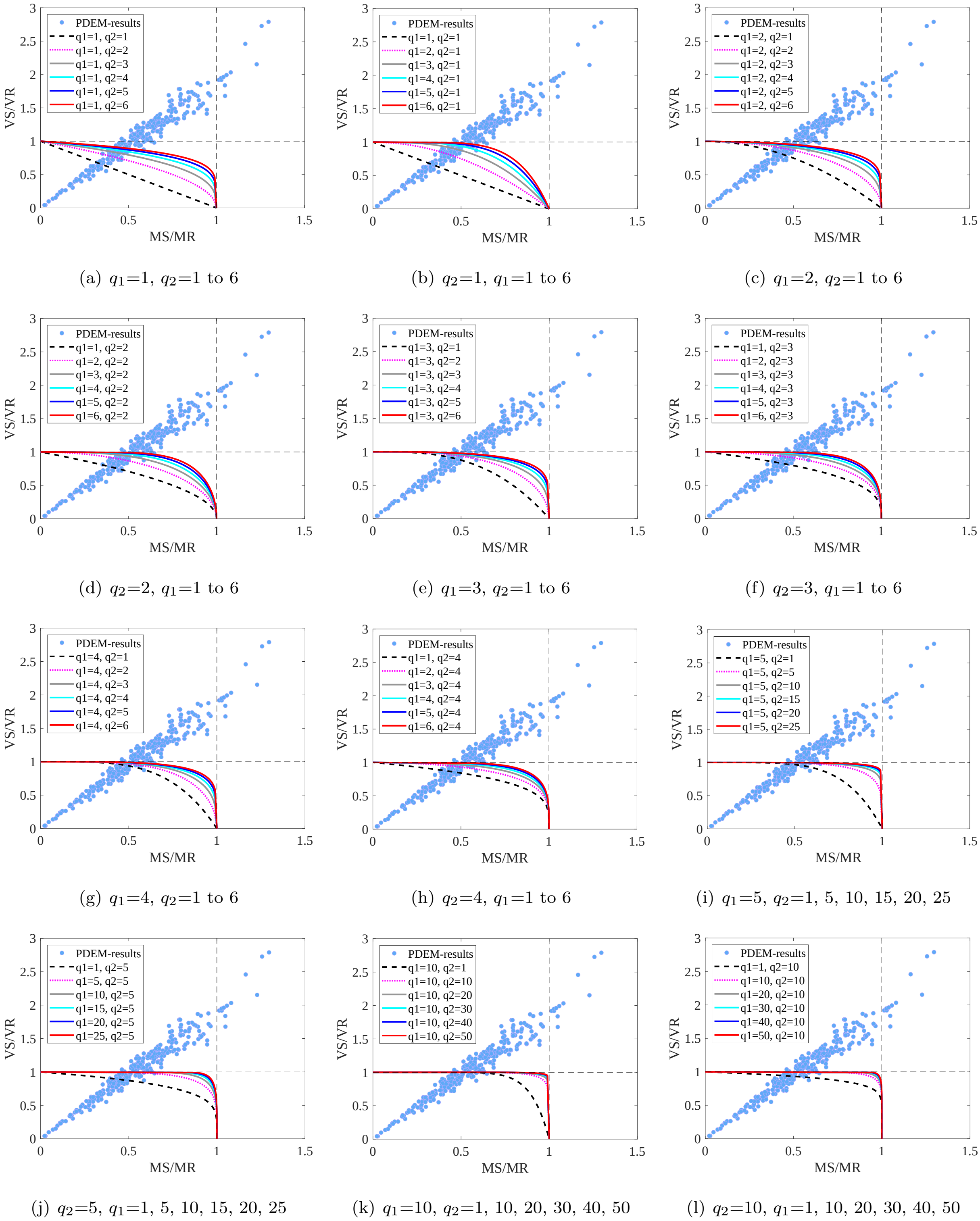

(a) q_1=1, q_2=1 to 6

(b) q_2=1, q_1=1 to 6

(c) q_1=2, q_2=1 to 6

(d) q_2=2, q_1=1 to 6

(e) q_1=3, q_2=1 to 6

(f) q_2=3, q_1=1 to 6

(g) q_1=4, q_2=1 to 6

(h) q_2=4, q_1=1 to 6

(i) q_1=5, q_2=1, 5, 10, 15, 20, 25

(j) q_2=5, q_1=1, 5, 10, 15, 20, 25

(k) q_1=10, q_2=1, 10, 20, 30, 40, 50

(l) q_2=10, q_1=1, 10, 20, 30, 40, 50

Figure 13: The schematic view of different LSFs and combination types in case study 1 (two failure modes)

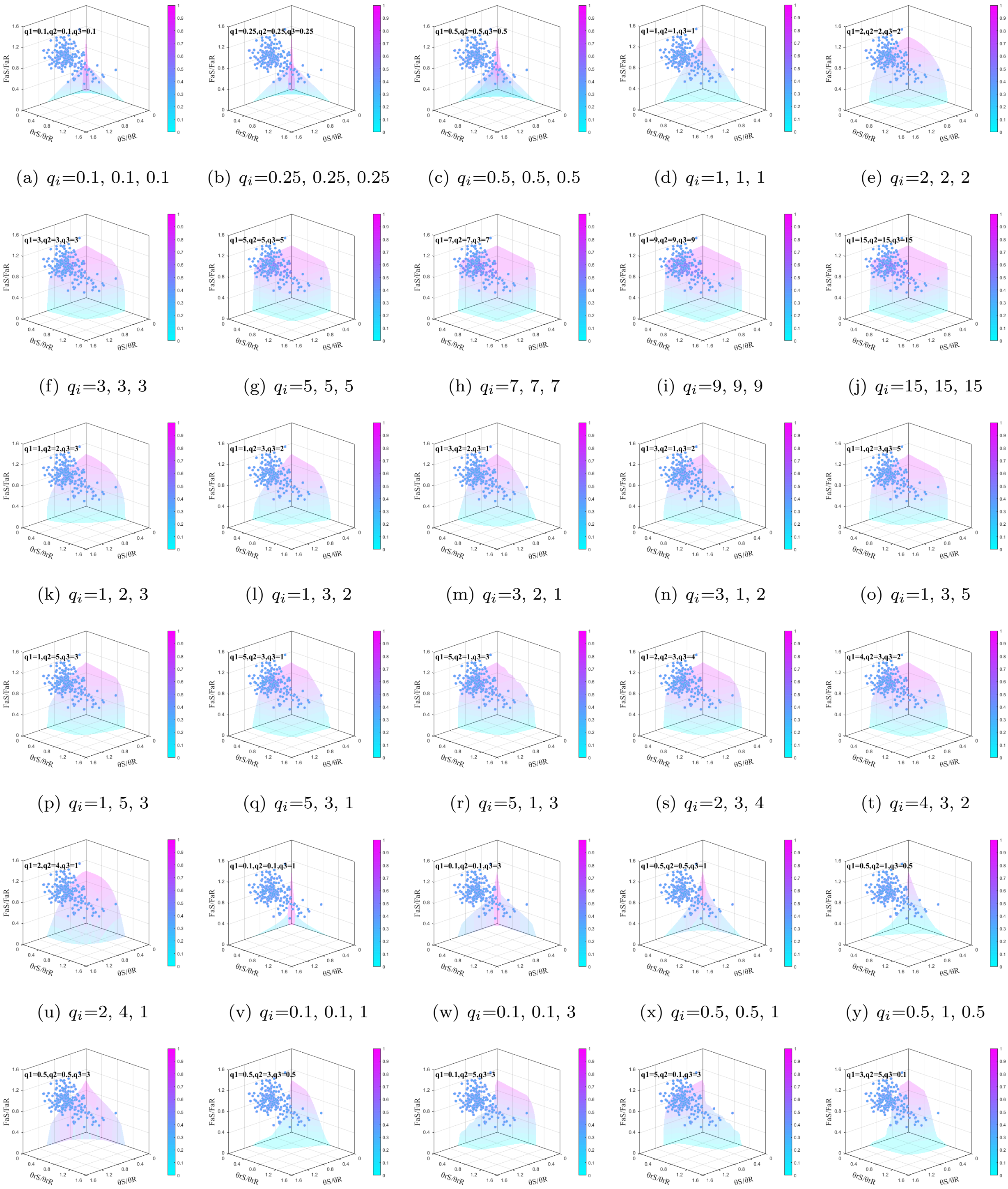

(a) q_i=0.1, 0.1, 0.1 (b) q_i=0.25, 0.25, 0.25 (c) q_i=0.5, 0.5, 0.5 (d) q_i=1, 1, 1 (e) q_i=2, 2, 2

(f) q_i=3, 3, 3 (g) q_i=5, 5, 5 (h) q_i=7, 7, 7 (i) q_i=9, 9, 9 (j) q_i=15, 15, 15

(k) q_i=1, 2, 3 (l) q_i=1, 3, 2 (m) q_i=3, 2, 1 (n) q_i=3, 1, 2 (o) q_i=1, 3, 5

(p) q_i=1, 5, 3 (q) q_i=5, 3, 1 (r) q_i=5, 1, 3 (s) q_i=2, 3, 4 (t) q_i=4, 3, 2

(u) q_i=2, 4, 1 (v) q_i=0.1, 0.1, 1 (w) q_i=0.1, 0.1, 3 (x) q_i=0.5, 0.5, 1 (y) q_i=0.5, 1, 0.5

(z) q_i=0.5, 0.5, 3 (aa) q_i=0.5, 3, 0.5 (ab) q_i=0.1, 5, 3 (ac) q_i=5, 0.1, 3 (ad) q_i=3, 5, 0.1

Figure 14: The schematic view of different LSFs and combination types in case study 2 (three failure modes)

5. Conclusions

In this paper, an enhanced PDEM-based framework considering multiple limit states and failure modes is proposed for reliability analysis of structures. The enhanced principle of the PDEM procedure is illustrated for guidance, two case studies with different failure combinations are given for validation, and parametric studies with related to two important aspects (modification and combination) are primarily performed for discussion, among which the following conclusions may be drawn:

1. The enhanced PDEM-based reliability framework commonly results in a more conservative result and is beneficial for a more comprehensive conclusion. For the first example, two failure modes are considered (i.e, flexural mode and shear mode), and for the seconde example, three failure modes are considered (i.e., MIDR mode, RIDE mode, PFA mode). In both examples, three combination ways (i.e., circle, triangle, and square ways) are specifically analyzed. After incorporating multiple limit states and multiple failure modes into the PDEM, the obtained results are more conservative and the calculated reliability is commonly lower than the single condition. The drop in reliability mainly results from the different combinations of failure modes as criterion, and multiple limit states significantly raise the threshold for the reliability requirement. Besides, with different combination ways of failure modes in LSFs, the obtained reliability presents variation within a certain range. In a sense, after incorporating the multiple limit states and different failure conditions, the obtained result can be more comprehensive and convincing, especially for a more robust decision making under the same condition in the practical engineering.

2. The enhanced PDEM-based reliability framework greatly improves the calculation efficiency and simultaneously keeps the calculating accuracy. To verify the effectiveness and accuracy of the enhanced PDEM-based framework in reliability assessment after considering multiple limit states, MCS is also performed for both examples as a comparison, which is commonly adopted as a benchmark for crosscheck. Compared with the single condition, the reliability via MCS is also more conservative, accompanied with a lower value for multiple limit states and failure modes, as demonstrated in the results from the enhanced PDEM procedure. Besides, the comparison between the MCS and PDEM proves the accuracy of the enhanced PDEM framework, and little difference is observed for all the LSFs (maximum of 3.51% in case study 1 and 7.28% in case study 2). In general, the enhanced PDEM-based framework indicates the non-parametric characteristics, and can better reflect the real stochastic conditions in practical engineering as well as the accurate calculating results for reliability assessment. At the same time, only 300 representative points are generated in case study 1 and 200 representative points are generated in case study 2 for the PDEM, while 10000 points are adopted in both examples for the MCS, which signifies the great efficiency improvement in calculation via the enhanced PDEM-based framework to some extent.

3. The modified strategy in representative points and other multi-LSF combinations in the enhanced PDEM deserve in-depth exploration in the further study. Parametric studies with related to two important aspects in the enhanced PDEM-based framework are performed, including a modified equation of the target variable value via representative points incorporating the influence of individual quantile parameters (e.g., 16%, 50% and 84% quantile), as well as the other potential combination types in the enhanced PDEM-based framework (i.e., more than circle, triangle, square ways). Generally, the smaller quantile level for benchmark will increase the reliability result, and the larger quantile level for benchmark will decrease the reliability result. Besides, with the increase of coefficient q_i, the boundary failure limitation is elevated and the system is prone to be more reliable under the same condition (i.e., with a higher reliability). When q_i is large enough, the obtained result is close to the form of $max(\cdot)$ via the square combination. The parametric studies of the modification procedure and other combination types deserve further in-depth research (e.g., benchmark point optimization, quantile level determination, appropriate combination principle, optimal combination coefficient). The staged progress in this paper sheds some light for the boundary rule of multi-LSF in PDEM, and meanwhile provides some reference for the future work in the enhanced PDEM-based reliability framework.

Acknowledgements

The authors greatly appreciate the National Natural Science Foundation of China (Grant Nos. 52078119 and 51838004), the Zhi-Shan Scholarship from Southeast University, China Postdoctoral Science Foundation (Grant No. 2022M711028), Jiangsu Funding Program for Excellent Postdoctoral Talent (Grant No. 2022ZB187), and Natural Science Foundation of Jiangsu Province (Grant No. BK20220984).

References

[1] H.-C. Liu, L. Liu, N. Liu, Risk evaluation approaches in failure mode and effects analysis: A literature review, Expert systems with applications 40 (2) (2013) 828–838.

[2] I. P. Mitseas, M. Beer, Fragility analysis of nonproportionally damped inelastic mdof structural systems exposed to stochastic seismic excitation, Computers & Structures 226 (2020) 106129.

[3] X.-Y. Cao, D. Shen, D.-C. Feng, C.-L. Wang, Z. Qu, G. Wu, Seismic retrofitting of existing frame buildings through externally attached sub-structures: State of the art review and future perspectives, Journal of Building Engineering 57 (2022) 104904.

[4] C. A. Cornell, F. Jalayer, R. O. Hamburger, D. A. Foutch, Probabilistic basis for 2000 sac federal emergency management agency steel moment frame guidelines, Journal of structural engineering 128 (4) (2002) 526–533.

[5] A. Basudhar, S. Missoum, A. H. Sanchez, Limit state function identification using support vector machines for discontinuous responses and disjoint failure domains, Probabilistic Engineering Mechanics 23 (1) (2008) 1–11.

[6] H. Dai, H. Zhang, W. Wang, G. Xue, Structural reliability assessment by local approximation of limit state functions using adaptive markov chain simulation and support vector regression, Computer-Aided Civil and Infrastructure Engineering 27 (9) (2012) 676–686.

[7] S. H. Ghasemi, A. S. Nowak, Target reliability for bridges with consideration of ultimate limit state, Engineering Structures 152 (2017) 226–237.

[8] X.-Y. Cao, D.-C. Feng, G. Wu, Z. Wang, Experimental and theoretical investigations of the existing reinforced concrete frames retrofitted with the novel external sc-pbspc brbf sub-structures, Engineering Structures 256 (2022) 113982.

[9] G. P. Cimellaro, A. Reinhorn, Multidimensional performance limit state for hazard fragility functions, Journal of engineering mechanics 137 (1) (2011) 47–60.

[10] P. Ceresa, L. Petrini, R. Pinho, R. Sousa, A fibre flexure–shear model for seismic analysis of rc-framed structures, Earthquake Engineering & Structural Dynamics 38 (5) (2009) 565–586.

[11] F. Berahman, F. Behnamfar, Probabilistic seismic demand model and fragility estimates for critical failure modes of un-anchored steel storage tanks in petroleum complexes, Probabilistic Engineering Mechanics 24 (4) (2009) 527–536.

[12] C. Christopoulos, S. Pampanin, M. Nigel Priestley, Performance-based seismic response of frame structures including residual deformations part i: single-degree of freedom systems, Journal of Earthquake Engineering 7 (01) (2003) 97–118.

[13] C. M. Ramirez, E. Miranda, Significance of residual drifts in building earthquake loss estimation, Earthquake Engineering & Structural Dynamics 41 (11) (2012) 1477–1493.

[14] W.-C. Hsu, J. Ching, Evaluating small failure probabilities of multiple limit states by parallel subset simulation, Probabilistic Engineering Mechanics 25 (3) (2010) 291–304.

[15] Y. Liu, F.-H. Lee, S.-T. Quek, M. Beer, Modified linear estimation method for generating multi-dimensional multi-variate gaussian field in modelling material properties, Probabilistic Engineering Mechanics 38 (2014) 42–53.

[16] P.-L. Liu, A. Der Kiureghian, Multivariate distribution models with prescribed marginals and covariances, Probabilistic engineering mechanics 1 (2) (1986) 105–112.

[17] R. Ambartzumian, A. Der Kiureghian, V. Ohaniana, H. Sukiasiana, Multinormal probability by sequential conditioned importance sampling: theory and application, Probabilistic Engineering Mechanics 13 (4) (1998) 299–308.

[18] A. Der Kiureghian, J. Song, Multi-scale reliability analysis and updating of complex systems by use of linear programming, Reliability Engineering & System Safety 93 (2) (2008) 288–297.

[19] A. C. Estes, D. M. Frangopol, Bridge lifetime system reliability under multiple limit states, Journal of bridge engineering 6 (6) (2001) 523–528.

[20] K. Mackie, B. Stojadinović, Performance-based seismic bridge design for damage and loss limit states, Earthquake engineering & structural dynamics 36 (13) (2007) 1953–1971.

[21] A. D. Orcesi, D. M. Frangopol, S. Kim, Optimization of bridge maintenance strategies based on multiple limit states and monitoring, Engineering Structures 32 (3) (2010) 627–640.

[22] F. Biondini, D. M. Frangopol, Time-variant redundancy and failure times of deteriorating concrete structures considering multiple limit states, Structure and Infrastructure Engineering 13 (1) (2017) 94–106.

[23] S. M. Mojtabaei, J. Ye, I. Hajirasouliha, Development of optimum cold-formed steel beams for serviceability and ultimate limit states using big bang-big crunch optimisation, Engineering Structures 195 (2019) 172–181.

[24] M. A. Valdebenito, P. Wei, J. Song, M. Beer, M. Broggi, Failure probability estimation of a class of series systems by multidomain line sampling, Reliability Engineering & System Safety 213 (2021) 107673.

[25] J. Sohn, I. Choi, J. Kim, Development of limit states for seismic fragility assessment of piloti-type structures verified with observed damage data, Engineering Structures 251 (2022) 113562.

[26] B. Moller, M. Beer, W. Graf, A. Hoffmann, Possibility theory based safety assessment, Computer-Aided Civil and Infrastructure Engineering 14 (2) (1999) 81–91.

[27] M. Beer, Y. Zhang, S. T. Quek, K. K. Phoon, Reliability analysis with scarce information: Comparing alternative approaches in a geotechnical engineering context, Structural Safety 41 (2013) 1–10.

[28] J. Li, D.-C. Feng, X. Gao, Y. Zhang, Stochastic nonlinear behavior of reinforced concrete frames. i: Experimental inves-

tigation, Journal of Structural Engineering 142 (3) (2016) 04015162.

[29] X.-Y. Cao, G. Wu, D.-C. Feng, Z. Wang, H.-R. Cui, Research on the seismic retrofitting performance of rc frames using sc-pbspc brbf substructures, Earthquake Engineering & Structural Dynamics 49 (8) (2020) 794–816.

[30] X.-Y. Cao, D.-C. Feng, G. Wu, J.-G. Xu, Probabilistic seismic performance assessment of rc frames retrofitted with external sc-pbspc brbf sub-structures, Journal of Earthquake Engineering (2021) 1–24.

[31] L. Huang, S. Li, Z. Si, et al., Research on designing for flood risk based on advanced checking-point (jc) method, Environmental Engineering and Management Journal 13 (8) (2014) 2119–2124.

[32] Y. Zheng, P. Das, Improved response surface method and its application to stiffened plate reliability analysis, Engineering structures 22 (5) (2000) 544–551.

[33] M. Feischl, G. Gantner, D. Praetorius, Reliable and efficient a posteriori error estimation for adaptive iga boundary element methods for weakly-singular integral equations, Computer Methods in Applied Mechanics and Engineering 290 (2015) 362–386.

[34] S. Rebello, H. Yu, L. Ma, An integrated approach for system functional reliability assessment using dynamic bayesian network and hidden markov model, Reliability Engineering & System Safety 180 (2018) 124–135.

[35] M. Marseguerra, E. Zio, Monte carlo approach to psa for dynamic process systems, Reliability Engineering & System Safety 52 (3) (1996) 227–241.

[36] L. Faravelli, Response-surface approach for reliability analysis, Journal of Engineering Mechanics 115 (12) (1989) 2763–2781.

[37] O. Ditlevsen, T. Arnbjerg-Nielsen, Model-correction-factor method in structural reliability, Journal of engineering mechanics 120 (1) (1994) 1–10.

[38] P. K. Das, Y. Zheng, Cumulative formation of response surface and its use in reliability analysis, Probabilistic Engineering Mechanics 15 (4) (2000) 309–315.

[39] W.-H. Kang, J. Song, P. Gardoni, Matrix-based system reliability method and applications to bridge networks, Reliability Engineering & System Safety 93 (11) (2008) 1584–1593.

[40] H. Jensen, D. Jerez, M. Valdebenito, An adaptive scheme for reliability-based global design optimization: A markov chain monte carlo approach, Mechanical Systems and Signal Processing 143 (2020) 106836.

[41] L.-L. Liu, Y.-M. Cheng, Q.-J. Pan, D. Dias, Incorporating stratigraphic boundary uncertainty into reliability analysis of slopes in spatially variable soils using one-dimensional conditional markov chain model, Computers and Geotechnics 118 (2020) 103321.

[42] D.-C. Feng, Y.-P. Liang, X. Ren, J. Li, Random fields representation over manifolds via isometric feature mapping-based dimension reduction, Computer-Aided Civil and Infrastructure Engineering 37 (5) (2022) 593–611.

[43] J. Li, J. Chen, The principle of preservation of probability and the generalized density evolution equation, Structural Safety 30 (1) (2008) 65–77.

[44] J. Li, Z. Liu, J. Chen, Orthogonal expansion of ground motion and pdem-based seismic response analysis of nonlinear structures, Earthquake Engineering and Engineering Vibration 8 (3) (2009) 313–328.

[45] J. Li, J. Chen, W. Sun, Y. Peng, Advances of the probability density evolution method for nonlinear stochastic systems, Probabilistic Engineering Mechanics 28 (2012) 132–142.

[46] J. Li, Probability density evolution method: background, significance and recent developments, Probabilistic Engineering Mechanics 44 (2016) 111–117.

[47] J. Chen, J. Yang, J. Li, A gf-discrepancy for point selection in stochastic seismic response analysis of structures with uncertain parameters, Structural Safety 59 (2016) 20–31.

[48] J. Li, J. B. Chen, J. Y. Yang, Pdem-based perspective to probabilistic seismic response analysis and design of earthquake-resistant engineering structures, Natural Hazards Review 18 (1) (2017) B4016002.

[49] W. Liu, Z. Li, Z. Song, J. Li, Seismic reliability evaluation of gas supply networks based on the probability density evolution method, Structural safety 70 (2018) 21–34.
[50] J. Chen, S. Yuan, Pdem-based dimension-reduction of fpk equation for additively excited hysteretic nonlinear systems, Probabilistic Engineering Mechanics 38 (2014) 111–118.
[51] W. Liu, Z. Song, Z. Wan, J. Li, Lifecycle operational reliability assessment of water distribution networks based on the probability density evolution method, Probabilistic Engineering Mechanics 59 (2020) 103037.
[52] D. Wang, W. Sun, J. Li, An rkpm-based formulation of the generalized probability density evolution equation for stochastic dynamic systems, Probabilistic Engineering Mechanics 66 (2021) 103152.
[53] J. Yang, J. Chen, H. Jensen, Structural design optimization under dynamic reliability constraints based on the probability density evolution method and highly-efficient sensitivity analysis, Probabilistic Engineering Mechanics 68 (2022) 103205.
[54] J. Xu, A pdem based new methodology for stochastic dynamic stability control of nonlinear structures with fractional-type viscoelastic dampers, Journal of Sound and Vibration 362 (2016) 16–38.
[55] W. Fan, A. H.-S. Ang, Z. Li, Reliability assessment of deteriorating structures using bayesian updated probability density evolution method (pdem), Structural Safety 65 (2017) 60–73.
[56] H. Hu, Y. Huang, Pdem-based stochastic seismic response analysis of sites with spatially variable soil properties, Soil Dynamics and Earthquake Engineering 125 (2019) 105736.
[57] D.-C. Feng, S.-C. Xie, J. Xu, K. Qian, Robustness quantification of reinforced concrete structures subjected to progressive collapse via the probability density evolution method, Engineering Structures 202 (2020) 109877.
[58] Z. Wan, J. Chen, J. Li, A. H.-S. Ang, An efficient new pdem-com based approach for time-variant reliability assessment of structures with monotonically deteriorating materials, Structural Safety 82 (2020) 101878.
[59] J. Chen, Q. Jia, Q. Xu, S. Fan, P. Liu, The pdem-based time-varying dynamic reliability analysis method for a concrete dam subjected to earthquake, in: Structures, Vol. 33, Elsevier, 2021, pp. 2964–2973.
[60] T. Zhou, Y. Peng, Active learning and active subspace enhancement for pdem-based high-dimensional reliability analysis, Structural Safety 88 (2021) 102026.
[61] X.-Y. Cao, D.-C. Feng, G. Wu, Pushover-based probabilistic seismic capacity assessment of rcfs retrofitted with pbspc brbf sub-structures, Engineering Structures 234 (2021) 111919.
[62] P. D. Spanos, M. Beer, J. Red-Horse, Karhunen–loève expansion of stochastic processes with a modified exponential covariance kernel, Journal of Engineering Mechanics 133 (7) (2007) 773–779.
[63] L. Comerford, I. A. Kougioumtzoglou, M. Beer, Compressive sensing based stochastic process power spectrum estimation subject to missing data, Probabilistic Engineering Mechanics 44 (2016) 66–76.
[64] I. P. Mitseas, I. A. Kougioumtzoglou, A. Giaralis, M. Beer, A novel stochastic linearization framework for seismic demand estimation of hysteretic mdof systems subject to linear response spectra, Structural Safety 72 (2018) 84–98.
[65] Z. Liu, W. Liu, Y. Peng, Random function based spectral representation of stationary and non-stationary stochastic processes, Probabilistic Engineering Mechanics 45 (2016) 115–126.
[66] Z. Liu, Z. Liu, D. Chen, Probability density evolution of a nonlinear concrete gravity dam subjected to nonstationary seismic ground motion, Journal of Engineering Mechanics 144 (1) (2018) 04017157.
[67] FEMA (Federal Emergency Management Agency). (2000). Commentary for the seismic rehabilitation of buildings (FEMA-356), Washington, DC.
[68] Hazus-MH, Multi-hazard loss estimation methodology: Earthquake model, Department of Homeland Security, FEMA, Washington, DC (2003) 235–260.
[69] X.-Y. Cao, D.-C. Feng, G. Wu, Seismic performance upgrade of rc frame buildings using precast bolt-connected steel-plate reinforced concrete frame-braces, Engineering Structures 195 (2019) 382 – 399.
[70] F. McKenna, G. L. Fenves, M. H. Scott, et al., Open system for earthquake engineering simulation, University of California,

Berkeley, CA.

[71] S. Mazzoni, F. McKenna, M. H. Scott, G. L. Fenves, et al., Opensees command language manual, Pacific Earthquake Engineering Research (PEER) Center, Berkeley, CA.

[72] T. Haukaas, Unified reliability and design optimization for earthquake engineering, Probabilistic Engineering Mechanics 23 (4) (2008) 471–481.

[73] Y. Bai, Y. Li, Z. Tang, M. Bittner, M. Broggi, M. Beer, Seismic collapse fragility of low-rise steel moment frames with mass irregularity based on shaking table test, Bulletin of Earthquake Engineering 19 (6) (2021) 2457–2482.

[74] D.-C. Feng, X.-D. Ren, Enriched force-based frame element with evolutionary plastic hinge, Journal of Structural Engineering 143 (10) (2017) 06017005.

[75] L. Huang, Z. Zhou, Y. Wei, Q. Xie, X. Sun, Seismic performance and resilience assessment of friction damped self-centering prestressed concrete frames, Engineering Structures 263 (2022) 114346.

[76] H.-J. Im, H.-G. Park, T.-S. Eom, Cyclic loading test for reinforced-concrete-emulated beam-column connection of precast concrete moment frame., ACI Structural Journal 110 (1).

[77] D.-C. Feng, G. Wu, Y. Lu, Finite element modelling approach for precast reinforced concrete beam-to-column connections under cyclic loading, Engineering Structures 174 (2018) 49–66.

[78] D. Feng, X. Ren, J. Li, Stochastic damage hysteretic model for concrete based on micromechanical approach, International Journal of Non-Linear Mechanics 83 (2016) 15–25.

[79] X.-Y. Cao, G. Wu, J.-W. W. Ju, Seismic performance improvement of existing rcfs using external pt-pbspc frame substructures: Experimental verification and numerical investigation, Journal of Building Engineering 46 (2022) 103649.

[80] X.-Y. Cao, D.-C. Feng, Z. Wang, G. Wu, Parametric investigation of the assembled bolt-connected buckling-restrained brace and performance evaluation of its application into structural retrofit, Journal of Building Engineering (2022) 103988.

[81] X.-Y. Cao, C.-Z. Xiong, D.-C. Feng, G. Wu, Dynamic and probabilistic seismic performance assessment of precast prestressed reinforced concrete frames incorporating slab influence through three-dimensional spatial model, Bulletin of Earthquake Engineering (2022) 1–35.

[82] J. Xu, D.-C. Feng, Seismic response analysis of nonlinear structures with uncertain parameters under stochastic ground motions, Soil Dynamics and Earthquake Engineering 111 (2018) 149–159.

[83] M. Barbato, Q. Gu, J. Conte, Probabilistic push-over analysis of structural and soil-structure systems, Journal of structural engineering 136 (11) (2010) 1330–1341.

[84] X. Yu, Probabilistic seismic fragility and risk analysis of reinforced concrete frame structures, Ph.D thesis of Harbin Institute of Technology, China.

[85] F. Nishino, A. Hasegawa, C. Miki, Y. Fujino, A fractile-based reliability structural design, in: Proceedings of the Japan Society of Civil Engineers, Vol. 1982, Japan Society of Civil Engineers, 1982, pp. 141–153.

[86] P. Hall, J. Strutt, Probabilistic physics-of-failure models for component reliabilities using monte carlo simulation and weibull analysis: a parametric study, Reliability Engineering & System Safety 80 (3) (2003) 233–242.

[87] M. A.-B. Abdo, Parametric study of using only static response in structural damage detection, Engineering Structures 34 (2012) 124–131.